

A deep near-infrared spectroscopic survey of the Scutum-Crux arm for Wolf-Rayet stars^{*}

C. K. Rosslowe and Paul A. Crowther[†]

Dept of Physics and Astronomy, University of Sheffield, Hicks Building, Hounsfield Road, Sheffield, S3 7RH, United Kingdom

14 September 2018

ABSTRACT

We present an NTT/SOFI spectroscopic survey of infrared selected Wolf-Rayet candidates in the Scutum-Crux spiral arm ($298^\circ \leq l \leq 340^\circ$, $|b| \leq 0.5^\circ$). We obtained near-IR spectra of 127 candidates, revealing 17 Wolf-Rayet stars – a $\sim 13\%$ success rate – of which 16 are newly identified here. The majority of the new Wolf-Rayet stars are classified as narrow-lined WN5–7 stars, with 2 broad-lined WN4–6 stars and 3 WC6–8 stars. The new stars, with distances estimated from previous absolute magnitude calibrations, have no obvious association with the Scutum-Crux arm. Refined near-infrared (YHJK) classification criteria based on over a hundred Galactic and Magellanic Cloud WR stars, providing diagnostics for hydrogen in WN stars, plus the identification of WO stars and intermediate WN/C stars. Finally, we find that only a quarter of WR stars in the survey region are associated with star clusters and/or H II regions, with similar statistics found for Luminous Blue Variables in the Milky Way. The relative isolation of evolved massive stars is discussed, together with the significance of the co-location of LBVs and WR stars in young star clusters.

Key words: stars: emission-line – stars: Wolf-Rayet – stars: evolution – galaxy: stellar content – infrared: stars.

1 INTRODUCTION

Wolf-Rayet (WR) stars – the progeny of massive O-type stars – are excellent tracers of young stellar populations in galaxies owing to their unique spectroscopic signatures of strong, broad emission lines (Crowther 2007). However, whilst WR surveys of nearby galaxies are nearing completeness (Massey et al. 2014), the Wolf-Rayet content of the Milky Way remains woefully incomplete (e.g. Shara et al. 2009) due to high dust obscuration at visual wavelengths. Our detailed knowledge of the evolution of massive stars remains unclear, with inaccuracies in earlier evolutionary phases magnified in the WR phase.

In addition, it is becoming clear that the conventional view of $\geq 20\text{--}25 M_\odot$ O stars advancing through the Luminous Blue Variable (LBV) stage en route to the nitrogen- (WN) and carbon- (WC) sequence Wolf-Rayet phase and ultimately a stripped envelope core-collapse supernova (ccSN) is incomplete if not incorrect. First, a high fraction of massive stars are now known to be multiple (Sana et al. 2012), so the major effects of close binary evolution needs to be considered. Second, it has been proposed that LBVs are lower

mass binary products, from an inspection of their spatial location in the Milky Way and Large Magellanic Cloud (LMC) with respect to Wolf-Rayet and O stars (Smith & Tombleson 2015). Third, Sander et al. (2012) argue from a spectroscopic analysis of Milky Way WC stars that the most massive stars do not pass through this phase. Finally, it is not clear whether the most massive stars will undergo a bright SN explosion after core-collapse, since they may collapse directly to a black hole or produce a faint SN and fallback to a black hole (Langer 2012).

Still, our Galaxy contains the largest *spatially resolved* population of WR stars, predicted to number ~ 1200 (Rosslowe & Crowther 2015a,b, hereafter RC15). The confirmed population has doubled over the previous decade, and currently stands at $\sim 640^1$. The Galactic disk therefore presents a rich hunting ground for further discoveries. Due to the large foreground interstellar dust extinction towards stars in the galactic disk, near and mid- infrared surveys are required.

The dense, ionized stellar wind of WR stars facilitate two approaches to infrared surveys. First, their strong, broad emission lines are amenable to near-IR narrow-band imaging (Shara et al. 2009, 2012; Kanarek et al. 2015). Second, their

^{*} Based on observations with ESO telescopes at the La Silla Paranal Observatory under programme 094.D-0839(A)

[†] Email: paul.crowther@sheffield.ac.uk

¹ <http://pacrowther.staff.shef.ac.uk/WRcat/>

dense winds exhibit a free-free excess leading to unusual infrared colours, which have been exploited in the near-IR (Homeier et al. 2003; Hadfield et al. 2007) and mid-IR (Mauerhan et al. 2011; Messineo et al. 2012; Faherty et al. 2014). To date, the majority of spectroscopic follow-up has been carried out to an approximate depth of $K_S \lesssim 11$ mag. However, the (coarse) model of the Galactic Wolf-Rayet distribution developed by RC15 suggests follow-up spectroscopy is needed to $K_S \sim 13$ mag in order to sample the majority of Wolf-Rayet stars.

Here we exploit prior photometric approaches to spectroscopically survey a region of the Galactic disk to fainter limits than to date ($K_S \sim 13$ mag). This has two interrelated goals: 1) the refinement and development of techniques that can be used to classify Wolf-Rayet stars using only infrared spectroscopy; 2) comprehensive searches for Wolf-Rayet stars in the Milky Way to allow more robust comparisons between their spatial locations and other massive stars; longer term goals involve the second data release (DR2) of *Gaia* which will provide parallaxes for hundreds of Wolf-Rayet stars, permitting their use as tracers of Galactic structure, and will be combined with upcoming large fibre-fed spectroscopic surveys, including WHT/WEAVE (Dalton et al. 2016) and VISTA/4MOST (de Jong et al. 2016).

This paper is structured as follows. In Section 2, we describe our photometric selection criteria and survey region, namely the Scutum-Crux spiral arm, the tangent to which lies at approximately $l \simeq 310^\circ$ (Georgelin & Georgelin 1976). Spectroscopic observations of Wolf-Rayet candidates, plus some previously known Galactic WR templates, are presented in Section 3, including a brief description of non-WR stars. Refined near-IR classification criteria for Wolf-Rayet stars are presented in Section 4. Results for newly identified WR stars are presented in Section 5, including distance estimates. We consider the spatial location of Wolf-Rayet and other massive stars in Section 6, including discussion of prior inferences about the nature of Luminous Blue Variables. Finally, in Section 7 we reflect on the low success rate of the methodology employed, and share some motivating points for future IR surveys targeting WR stars.

2 CANDIDATE SELECTION

Here we discuss our selection of sight lines towards the Scutum-Crux arm, plus our photometric criteria for the selection of candidate Wolf-Rayet stars. Specifically, we focus on $l = 298\text{--}340^\circ$, which Russeil et al. (2005) have previously highlighted in determining Galactic structure, since this intersects three proposed spiral arm features – Sagittarius-Carina, Scutum-Crux and Norma-Cygnus (Russeil 2003, their Fig. 5). The majority of known Wolf-Rayet stars in this region lie at distances < 6 kpc, consistent with the nearby Sagittarius-Carina arm. However, assuming typical $M_{K_S} = -5$ and $A_{K_S} = 2$ for Galactic WR stars, it is possible to probe heliocentric distances 6–15 kpc by identifying WR stars in the magnitude range $K_S = 11\text{--}13$ mag. Therefore WR stars may provide a comparable and complimentary tracer of Galactic structure to commonly used non-stellar objects, i.e., H II regions and atomic H gas. We confined our search to latitudes $|b| < 0.5^\circ$, ensuring that at the furthest expected distances, candidate WR stars remain within a few

scale heights of the Galactic plane (FWHM=80 pc for WRs, RC15).

We selected candidate Wolf-Rayet stars for which $298^\circ \leq l \leq 340^\circ$ and $|b| \leq 0.5^\circ$ from their near-IR (2MASS Skrutskie et al. 2006) and mid-IR (GLIMPSE-I Benjamin et al. 2003) photometry. We limited our survey to GLIMPSE-I point sources with a corresponding 2MASS detection², requiring a minimum 2MASS quality flag of ‘C’ in the K_S filter, and rejected sources with one or more Source Quality Flags $> 10^5$ in the GLIMPSE-I catalogue. We then used the TOPCAT³ tool to apply various cuts in colour and magnitude.

Mauerhan et al. (2011) identified several regions of colour space (their grey shaded region in Fig. 1) favoured by Wolf-Rayet stars, which we have adapted as follows:

$$\begin{aligned} 1.25(K_S - [8.0]) &\leq (J - K_S) + 0.5 < 2.5(K_S - [8.0]), \\ K_S - [8.0] &\geq 1.3, \\ 0.8 &\leq ([3.6] - [8.0]) \leq 1.6, \\ 0.3 &\leq ([3.6] - [4.5]) \leq 0.75. \end{aligned}$$

In addition, Messineo et al. (2012) introduced additional reddening-free parameters $Q1 = (J - H) - 1.8(H - K_S)$ and $Q2 = (J - K_S) - 2.69(K - [8.0])$ which we also utilise:

$$(11.25Q1 - 2.38) < Q2 < -1.0.$$

It is necessary to emphasise that not all WR stars occupy this parameter space, although there is no bias towards either WN or WC subtypes. Still, some dusty WC stars are offset from the majority of WR stars in the $J\text{--}K_S$ vs $K_S - [8.0]$ colour colour diagram (Mauerhan et al. 2011, their Fig. 1), so our survey criteria are potentially biased against such stars. Approximately 250 sources satisfied these criteria. We subsequently cross-checked the co-ordinates of these with the SIMBAD⁴ database, to find any with previous identifications. Encouragingly, 14% of these were known WR stars (23% of known WRs in the survey area), 4% had non-WR classifications (mostly Be stars or young stellar objects), leaving ~ 200 candidates with no previous spectral classification. Colour-colour diagrams for 191 candidates involving $K_S - [8.0]$ vs $(J - K_S)$ and $[3.6] - [8.0]$ vs $[3.6] - [4.5]$ are presented in Figure 1 together with reddening-free parameters $Q1$ and $Q2$ from Messineo et al. (2012).

3 NTT/SOFI SPECTROSCOPY OF WOLF-RAYET CANDIDATES

We obtained near-IR spectroscopy of 127 WR candidates between 29–31 March 2015 (program ID 094.D-0839) using the Son-of-Isaac (SOFI) spectrograph at the New Technology Telescope (NTT). These represent 66% of the IR selected candidates presented in Fig. 1. Candidates were observed with the red grism (GR) covering the $1.53\text{--}2.52\mu\text{m}$ spectral region, a dispersion of $10.2\text{\AA}/\text{pix}$, and a slit width of 1 arcsec, providing a spectral resolution of $R \sim 600$. All sources were observed using a standard ABBA sequence, including

² via the IPAC/NASA Infrared Science Archive: <http://irsa.ipac.caltech.edu>

³ Available at: <http://www.starlink.ac.uk/topcat/>

⁴ <http://simbad.u-strasbg.fr/simbad/>

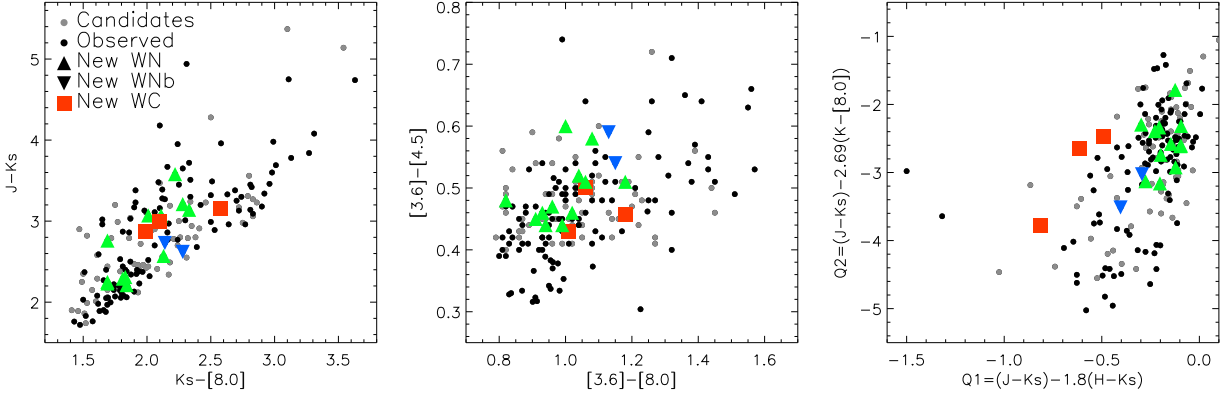


Figure 1. Colour-colour diagrams from 2MASS and GLIMPSE-I, showing 191 candidates in our survey area (circles) we obtained NTT/SOFI HK spectra for 127 stars (black), leaving 64 unobserved (grey). Newly discovered WR stars are indicated: triangles for WN stars and squares for WC stars. The left panel shows $K_S-[8.0]$ versus $J-K_S$, central panel indicates $[3.6]-[8.0]$ versus $[3.6]-[4.5]$ while the right panel presents the reddening free parameters $Q1$ versus $Q2$ from [Messineo et al. \(2012\)](#).

Table 1. Catalogue of newly identified Wolf-Rayet stars, including WR75-30 (1083–1765) from [Kanarek et al. \(2015\)](#)

ID	WR Number	RA – J2000 –	Dec	l	b	K_S mag	$J-K_S$ mag	$H-K_S$ mag	$K_S-[3.6]$ mag	$[3.6]-[4.5]$ mag	$K_S-[8.0]$ mag	SOFI Grisms	Spectral Type
E#3	WR46-18	12:08:52.49	–62:50:54.9	298.0981	–0.3769	10.47	2.87	1.20	0.80	0.46	1.98	GB,GR	WC6-7
B#13	WR47-5	12:50:48.98	–62:24:39.8	302.8599	+0.4606	11.09	2.23	0.83	0.70	0.44	1.69	GB,GR	WN6(h)
B#37	WR56-1	13:41:50.01	–62:20:25.8	308.7434	–0.0387	12.18	2.76	1.03	0.87	0.48	1.69	GB,GR	WN5o
B#51	WR60-7	14:02:33.44	–61:20:27.2	311.3533	+0.3626	10.28	3.00	1.29	1.09	0.43	2.10	GB,GR	WC7-8
B#56	WR60-8	14:12:15.19	–61:42:45.2	312.3517	–0.3277	11.76	3.14	1.22	1.15	0.51	2.33	GB,GR	WN6o
B#85	WR64-2	15:01:14.05	–58:49:07.4	319.0607	–0.0724	11.89	2.57	0.99	1.07	0.51	2.13	GB,GR	WN6o
B#87	WR64-3	15:02:46.14	–58:27:06.5	319.4120	+0.1535	10.18	2.21	0.86	0.88	0.47	1.84	GB,GR	WN6o
B#88	WR64-4	15:04:11.15	–58:27:21.5	319.5721	+0.0601	9.10	2.25	0.91	0.76	0.46	1.69	GB,GR	WN6o+OB
B#91	WR64-5	15:07:31.84	–58:15:09.6	320.0540	+0.0209	10.80	2.31	0.86	0.89	0.44	1.83	GB,GR	WN6o
B#93	WR64-6	15:10:57.65	–57:57:28.5	320.5939	+0.0474	11.11	2.73	1.08	0.99	0.54	2.14	GB,GR	WN6b
B#105	WR70-13	15:37:46.51	–56:08:45.2	324.6325	–0.4487	9.96	3.16	1.42	1.52	0.50	2.58	GB,GR	WC8d
B#107	WR70-14	15:39:17.02	–55:49:18.9	324.9945	–0.3129	11.50	2.62	1.08	1.15	0.59	2.28	GB,GR	WN4b
B#123	WR70-15	15:58:57.97	–52:46:05.4	329.1414	+0.2865	12.40	3.21	1.19	1.20	0.58	2.28	GB,GR	WN5o
B#132	WR72-5	16:07:01.45	–51:58:18.3	330.5909	+0.0725	10.27	2.29	0.87	0.77	0.52	1.81	GB,GR	WN6o
A#11	WR75-31	16:25:13.60	–48:58:22.3	334.7557	+0.2255	12.21	3.07	1.13	1.09	0.46	2.11	GB,GR	WN7o
A#13	WR75-30	16:32:25.70	–47:50:45.8	336.3959	+0.1395	11.57	3.58	1.36	1.22	0.60	2.22	GR	WN7o
B#154	WR76-11	16:40:12.92	–46:08:54.0	338.5451	+0.2996	11.98	3.07	1.17	1.10	0.45	2.01	GR	WN7o

a small random offset in the A and B positions between exposures.

Before extracting 1D spectra, we subtracted a median dark frame from each individual frame, then subtracted adjacent AB pairs from one another. The result of this was 4 dark frame-corrected spectra for each source, free from sky lines. We extracted these 4 spectra for each object using IRAF. Wavelength calibration was performed using strong and isolated sky lines at known wavelengths ([Rousselot et al. 2000](#)) present in each raw frame, after which all spectra for each object were co-added.

Throughout each night, we periodically observed bright Vega-type telluric standard stars, at similar airmasses to the WR candidates. The removal of telluric spectral features was achieved using `telluric` in IRAF. We also used these telluric standards, together with Kurucz models of the same

spectral types, to perform relative flux calibration, which are subsequently adjusted to match 2MASS photometry.

Of the 127 candidates, 17 stars were identified as WR stars. Of these, one candidate was subsequently matched to the recently discovered WN6 star 1093-1765 (= WR75-30) from [Kanarek et al. \(2015\)](#), such that 16 stars are newly identified as WR stars in this study. Previous surveys of Wolf-Rayet stars from IR photometric criteria have achieved similar efficiencies ([Mauerhan et al. 2011](#); [Faherty et al. 2014](#)). We briefly discuss the nature of the non-WR stars in Sect. 3.1 and discuss the newly identified WR stars in Sect. 4. New WR stars are indicated in Fig. 1, with a subtype dependence apparent in the reddening-free $Q1$ vs $Q2$ diagram. Table 1 provides basic observational properties for the new Wolf-Rayet stars, for which we obtained NTT/SOFI spectroscopy, while Table B1 (available online) provides a list of all candidates for which we ob-

Table 2. Spectroscopic datasets exploited for the updated near-IR classification scheme

Tel/Inst	R	Spect Range	Epoch	Ref	Dataset/ Programme
CTIO 4m/IRS	3000	Y K	Mar 1996	a	C1
ESO 1.5m/B&C		Y	Feb 1982	b	E1
INT/IDS	3000	Y	Aug 1990	c	I1
Lick 3m/UCLA	525	K	1994-1995	d	L1
MSO/CGS	600-850	YJHK		e	M1
NTT/SOFI	1000	YJHK	Sep 1999	f	N1/63.H-0683
NTT/SOFI	600-1300	YJ K	May 2002	g	N2/69.B-0030
NTT/SOFI	600-1000	YJHK	Nov 2003		N3/71.D-0272
NTT/SOFI	600	YJ	Nov 2004		N4/74.D-0696
NTT/SOFI	600	YJHK	Jun 2005	h	N5/75.D-0469
NTT/SOFI	600	YJHK	Mar 2015	i	N6/94.D-0839
OHP/CARELEC		Y	Sep 1989	j	O1
UKIRT/CGS2	400-600	YJHK		k	U1
UKIRT/CGS4	1000-1400	HK	Jan 1994	l	U2
UKIRT/CGS4	600-850	YJHK	Aug 1994	m	U3
UKIRT/CGS4	1500	YJ K	Sep 1995		U4
UKIRT/CGS4	3000	K	May 1996	a	U5
UKIRT/CGS4	1500	YJ K	Apr 1997		U6
VLT/XSHOOTER	5000	YJHK	2013-2014	n	V1

a: (Bohannon & Crowther 1999), b: (Vreux et al. 1983);
c: (Howarth & Schmutz 1992), d: (Figer et al. 1997), e:
(Hillier et al. 1983), f: (Crowther 2000), g: (Homeier et al.
2003); h: (Crowther et al. 2006), i: This study; j: (Vreux et al.
1990), k: (Eenens et al. 1991), l: Crowther et al. (1995), m:
(Crowther & Smith 1996); n: (Tramper et al. 2015)

tained spectroscopy, together with a brief note describing the nature of each source.

In addition to the candidate WR stars, we have also obtained NTT/SOFI spectroscopy of 14 Wolf-Rayet stars for which optical classifications have been undertaken, in order to refine near-IR based classification criteria (see Sect. 4). Finally, we also obtained blue grism (GB) spectroscopy with SOFI for the majority of newly identified WR stars. The GB observations cover the spectral region 0.95–1.64 μm , a dispersion of 7.0 $\text{\AA}/\text{pix}$, and an identical slit width of 1 arcsec, again providing $R \sim 600$. Data reduction was undertaken in an identical manner to the GR datasets.

3.1 Non Wolf-Rayet stars

A significant subset of the 110 candidates that were not confirmed to be WR stars exhibited a hydrogen emission line spectrum, with Br γ observed in 60 (55%) cases, plus often higher Brackett series (Br10, 11), and He I 2.058 μm emission present in a quarter of instances. These sources are likely to be massive young stellar objects (mYSOs) or Herbig AeBe stars (see e.g. Porter et al. 1998; Cooper et al. 2013). Br γ emission equivalent widths are typically 10–30 \AA , with He I/Br γ ratios of 0.3–1. The majority of Br γ emission lines are unresolved (FWHM \sim 30 \AA) although several stars (e.g. B#127, 147, 149) possess broad emission (FWHM \sim 50–60 \AA). Unusually, B#66 exhibits strong He I 2.058 μm emission, without significant Br γ emission, warranting follow up observations.

Mid-IR imaging has revealed circumstellar ring nebu-

lae around many evolved stars (e.g., Wachter et al. 2010; Toalá et al. 2015). Such nebulae appear prominently in Spitzer 8.0 μm images, owing to thermal emission from dust swept up by stellar winds. Mindful of this, we inspected 5' \times 5' Spitzer 8.0 μm images centred on all candidates. One of the Br γ emission line sources, A#9 (SSTGLMC G330.7900-00.4539), is the central star of a striking oval mid-IR ring nebula, S65, which was identified by Churchwell et al. (2006) and studied by Simpson et al. (2012).

Strong absorption lines in the Brackett series are observed in one candidate, B#3, indicating an A- or late-B type star, with Br γ absorption observed in another object, B#54, albeit without other prominent features suggesting an early type star in this instance. Four candidates – B#21, B#100, B#122 and B#153 – exhibit prominent CO 2.3 μm bandhead absorption features, although none of these involve Br γ emission line sources, indicating a late-type star origin. The remaining 44 candidates (40% of the non WR stars) either have no prominent absorption or emission features, or the S/N achieved was insufficient to identify their nature.

4 NEAR-IR CLASSIFICATION OF WOLF-RAYET STARS

The switch from optical to near-IR spectroscopy for the overwhelming majority of new Galactic Wolf-Rayet stars requires a reassessment of spectral classification criteria. Vreux et al. (1990) provided a classification scheme based upon Y-band observations of northern WR stars, while Eenens et al. (1991) devised a near-IR scheme for WC stars from 1–5 μm spectroscopy. More recently Crowther et al. (2006, hereafter C06) provide near-IR classification diagnostics for WN and WC stars, based on equivalent width ratios. Qualitatively, early-type WC4–6 stars possess broader emission lines than later WC7–9 subtypes, although exceptions do exist (Eenens & Williams 1994).

An updated a quantitative near-IR classification of Wolf-Rayet stars is made feasible by access to a greatly expanded sample of Galactic and Magellanic Cloud WR stars for which optical classifications have been made, primarily Smith et al. (1996) for WN stars and Smith et al. (1990) for WC stars. The datasets utilised were drawn from various sources, primarily NTT/SOFI and UKIRT/CGS4, as summarised in Table 2. We have also inspected high resolution, intermediate resolution IRTF/SpeX spectroscopy of northern Galactic WR stars, provided by W.D. Vacca (priv. comm.), although we focus our criteria on moderate resolution ($R = 600 - 1000$), modest signal-to-noise spectroscopy in the 0.95 – 2.5 μm near infrared.

To date, no criteria for the identification of WN/C or WO stars from near-IR spectroscopy have been considered, nor has an attempt to distinguish between H-rich and H-deficient WN stars, although C06 did separate broad-lined WN stars (FWHM He II 1.01 μm \geq 65 \AA) from narrow-lined counterparts. In our revised near-IR classification scheme we attempt to utilise pairs of lines from adjacent ionization stages of helium for WN stars, and adjacent ionization stages of carbon for WC stars. In some instances nitrogen lines are required for WN stars, in common with C06, plus ratios of carbon to helium lines are

utilised for WN/C and WC stars, which will also depend upon their relative abundances. We omit from our discussion the near-IR classification of transition Of/WN stars, which has been considered by Bohannan & Crowther (1999) and Crowther & Walborn (2011). WN stars with intrinsic absorption features (WNh+abs, WNha) also offer specific challenges which will need to be considered separately.

A detailed description of the updated classification scheme is provided in Appendix A (available online), while we present a summary of Y, J, H and K-band classification diagnostics for WN, WN/C, WC and WO subtypes in Table 3. In Figs A1–A2 (available online) we present YJ-band and HK-band spectroscopy of template (optically classified) WN, WN/C, WC and WO stars, with line measurements provided in Tables A1–A3, also online. Overall, the use of solely IR diagnostics provide satisfactory classifications, although confidence in resulting spectral types requires multi-band spectral coverage, a minimum spectral resolution of $R \sim 500$ and moderate signal-to-noise. In many instances, observations at a single band prevent a refined classification. For example, WC4–7 stars may not be distinguished using solely K-band spectroscopy, while it is not possible to differentiate between broad-lined WN4–7 stars on the basis of low S/N spectroscopy in the Y-band. Still, reliable, Wolf-Rayet subtypes can be obtained from complete 1–2.5 μm spectroscopy, with the exception of broad-lined WN4–6 stars and WC5–6 stars. In addition, WO stars have a very distinctive near-IR spectrum, and WN/C stars possess characteristics in each of Y, J, H and K-bands which distinguish them from normal WN stars. In addition, the presence of hydrogen in WN stars can be identified in most subtypes, although very late subtypes are challenging since a low He II 1.163/P β or He II 2.189/Br γ ratio may indicate either a high hydrogen content or a low ionization atmosphere.

4.1 Robustness of near-IR classification

In order to assess the robustness of the new scheme, we reclassify several WN and WC stars which have been discovered and classified from red optical spectroscopy. We utilise NTT/SOFI spectroscopy of four WN stars, WR62a, WR68a, WR93a from Homeier et al. (2003) (dataset N2 in Table 2), plus WR75–30 from our own observations (dataset N5 in Table 2), together with three WC stars, WR107a from Homeier et al. (2003) plus WR75aa and WR75c from our own observations. Near-IR spectra are presented in Figs 2–3. Individual line measurements are provided in Table 4 and 5 for WN and WC stars, respectively, while line ratios are presented in Table 6. Measurements have employed Gaussian fits, using the `elf` suite of commands within the Starlink DIPSO package⁵.

4.1.1 WN stars

WR62a was classified as WN5o by Shara et al. (1999, their source #11), and we support its classification as a narrow-lined WN star. Consequently, the primary diagnostics are the He I 1.08/He II 1.01 μm ratio and K-band morphology. The former indicates a WN6 subtype, while He I + N III 2.11

> N v 2.10, favours a WN5–6 subtype. The P β /He II 1.16 μm ratio indicates WR62a is hydrogen-free, while the Br γ /He II 2.19 μm suggests a borderline o/(h) classification, so overall we favour WN6o for WR62a. The same arguments and ratios apply to WR68a for which Shara et al. (1999, their source #13) assigned WN6o. We support this classification owing to its morphological similarity to WR62a.

WR93a (Th 3–28), was originally classified as WN2.5–3 by Acker & Stenholm (1990) and revised to WN6 by Miszalski et al. (2013) from optical spectroscopy. This is also a narrow-lined WN star so again we focus on its He I 1.08/He II 1.01 μm ratio and K-band morphology. Both favour a WN6 subtype, with a significant hydrogen content from our multiple diagnostics (darker shaded regions in Fig. A4, available online), so we adopt WN6h for WR93a.

Kanarek et al. (2015, their source 1083-1765) originally classified WR75-30 as a WN6 star from near-IR spectroscopy. The He I 1.70/He II 1.69 μm ratio favours a WN7 subtype, as does (He I + N III 2.11)/He I 2.19 μm ~ 1 , while the Br γ /He II 2.19 μm ratio lies in the hydrogen-free region of Fig. A4 so we favour WN7o for this star.

4.1.2 WC stars

WR75aa and WR75c were identified as WC9 stars by Hopewell et al. (2005) from red optical spectroscopy. All our primary near-IR diagnostics support this assessment, as do the secondary criteria involving helium for WR75c. WR75aa has a borderline WC8–9 classification from the He I–II 1.7/C IV 1.74 μm ratio, but overall both stars are unambiguous WC9 stars.

Finally, WR107a (#18 from Shara et al. 1999) was originally classified as a WC6 star from red optical spectroscopy. Our primary criteria indicate the follow for WR107a: WC6 ± 1 from both C III 1.20/C IV 1.19 and C III 2.11/C IV 2.07, WC5–8 from C II 0.99/C III 0.97. Our secondary criteria indicate WC5 from He I 1.08/He II 1.01, and WC7 from C III 0.97/He II 1.01 μm (H-band spectra are unavailable), so although WC6 is plausible we provide a more cautious WC5–7 classification. Indeed, the primary optical diagnostic ratio (C III 5696/C IV 5808) also favoured WC6–7 according to Shara et al. (1999).

In general, the K-band is preferred to shorter wavelengths for classification of highly reddened WR stars, but K-band spectral features of dusty WC stars are often masked by host dust emission. Extremely high S/N is required to identify K-band spectral features of the Quintuplet Q stars. By way of example, Liermann et al. (2009) assign a WC8/9d+OB subtype to Q3 (WR102ha) from K-band spectroscopy, whereas WC features are relatively prominent in deep H- and J-band spectroscopy. We confirm a WC9d subtype for Q3 on the basis of high S/N Gemini spectroscopy presented by Najarro et al. (2015), owing to C III 1.20/C IV 1.19 $\gg 1$, C II 1.78/C IV 1.74 > 1 and C III 2.11/C IV 2.07 $\gg 1$.

⁵ Available at: <http://starlink.eao.hawaii.edu/starlink>

Table 3. Classification of Wolf-Rayet stars based on emission equivalent width ratios of diagnostics in the Y,J,H,K spectral regions, updated from C06, primary diagnostics in bold font. The majority of diagnostics are blended with other lines in broad-lined Wolf-Rayet stars, including O VI 1.075 with C IV 1.054 and He II 1.093, He I 1.083 with P γ , C IV 1.191 with C III 1.198, He II 1.692 with He I 1.700, C II 1.785 with C IV 1.801, C IV 2.070–2.080 with C III 2.115, and He II 2.189 with Br γ . For near-IR classification of transition Of/WN stars, see Bohannan & Crowther (1999) and/or Crowther & Walborn (2011).

Subtype	FWHM km s ⁻¹	Diagnostic Y-band	Diagnostic J-band	Diagnostic H-band	Diagnostic K-band	Notes	Templates
Narrow-lined WN stars (FWHM(He II 1.01μm) \lesssim 1900 km s⁻¹ and log Wλ(He II 1.01μm/\AA) \lesssim 2.5)							
WN Subtype	He II 1.012 μ m	log W λ (He I 1.08/ He II 1.01)	log W λ (P β / He II 1.16)	log W λ (He I 1.70/ He II 1.69)	log W λ (Br γ / He II 2.19)	Notes	Templates
9	300	≥ 1.4	~ 1.5 (h)	≥ 1.4	~ 1.5 (h)	He I+N III 2.11 \gg He II 2.19	WR105, BAT76
8	700	1.4\pm0.4	≤ 0.3 (o); ≥ 0.1 (h)	0.9\pm0.5	≤ 0.5 (o); ≥ 0.4 (h)	He I+N III 2.11 \gg He II 2.19	WR40, WR123
7	800	0.4\pm0.2	≤ 0 (o); ≥ 0 (h)	0.2\pm0.2	≤ 0.1 (o); ≥ 0.1 (h)	He I+N III 2.11 \sim He II 2.19	WR78, WR120
6	1200	0.0\pm0.2	≤ -0.1 (o); ≥ -0.1 (h)	~ -0.1	≤ -0.1 (o); ≥ -0.1 (h)	He II 2.19 $>$ He I+N III 2.11 \gg N v 2.10	WR115
5	1400	-0.3\pm0.1	≤ -0.2 (o); ≥ -0.2 (h)	~ -0.3	≤ -0.2 (o); ≥ -0.2 (h)	He II 2.19 \gg He I+N III 2.11 \geq N v 2.10	BAT122
4	1500	-0.7\pm0.3	≤ -0.3 (o); ≥ -0.3 (h)	~ -0.6	≤ -0.3 (o); ≥ -0.3 (h)	He II 2.19 \gg N v 2.10 $>$ He I+N III 2.11	WR128, BAT75
3	1600	≤ -1.0	≤ -0.4 (o); ≥ -0.4 (h)	≤ -0.8	≤ -0.4 (o); ≥ -0.4 (h)	He II 2.19 \gg N v 2.10 \gg He I+N III 2.11	WR46, WR152
Broad-lined WNb stars (FWHM(He II 1.01μm) \gtrsim 1900 km s⁻¹ and log Wλ(He II 1.01μm/\AA) \gtrsim 2.5)							
WN Subtype	He II 1.012 μ m	log W λ (He I 1.08/ He II 1.01)	log W λ (P β / He II 1.16)	log W λ (He I 1.70/ He II 1.69)	log W λ (Br γ / He II 2.19)	Notes	Templates
7	3300	≥ 0.2	-0.3 (o)	+0.4:	-0.2 (o)	He II 2.19 $>$ He I+N III 2.11	WR77sc
6	2600	+0.3\pm0.2	≤ -0.3 (o); ≥ -0.3 (h)	-0.3:	≤ -0.2 (o); ≥ -0.2 (h)	He II 2.19 \gg He I+N III 2.11 $>$ N v 2.10	WR75, WR134
4	2400	-0.5\pm0.5	≤ -0.3 (o)	-0.5:	≤ -0.2 (o); ≥ -0.2 (h)	He II 2.19 \gg He I+N III 2.11 \sim N v 2.10	WR6, WR18
2-3	2550	≤ -1	≤ -0.5 (o); ≥ -0.5 (h)	≤ -1.0	≤ -0.4 (o); ≥ -0.4 (h)	He II 2.19 \gg N v 2.10 \gg He I+N III 2.11	WR2, BAT51
WN/C stars							
WN/C Subtype		log W λ (C III 0.97/ He II 1.01)	log W λ (C IV 1.19/ He II 1.16)	log W λ (C IV 1.74/ He I-II 1.7)	log W λ (C IV 2.07/ He I+C III 2.11)	log W λ (C IV 2.43/ He II 2.34) Notes	Templates
All		-0.5	≥ -0.7	≥ -0.7	≥ -0.3	≥ 0	WR8, WR26
WC stars							
WC Subtype	He II 1.190 μ m	log W λ (He I 1.08/ He II 1.01)	log W λ (C III 1.20/ C IV 1.19)	log W λ (He I-II 1.7/ C IV 1.74)	log W λ (C III 2.11/ C IV 2.07)	log W λ (C II 0.99/ C III 0.97) Notes	Templates
9	850	+1.1	+0.6$^{+0.2}_{-0.5}$	$0.3^{+0.1}_{-0.5}$	+0.1\pm0.3	-1.1\pm0.2 C II 1.78 $>$ C IV 1.74	WR92, WR103
8	1800	+0.4 \pm 0.2	-0.2$^{+0.3}_{-0.2}$	-0.4 \pm 0.2	-0.35\pm0.1	-1.3\pm0.1	WR135
7	1900	+0.2 \pm 0.2	-0.5\pm0.1	-0.7 \pm 0.1	-0.6$^{+0.2}_{-0.15}$	-1.35\pm0.15	WR90
6	2900	+0.2	-0.7\pm0.2	-0.8 \pm 0.1	-0.7\pm0.1	-1.6\pm0.1	WR15, WR23
5	2300	+0.0	-0.6\pm0.1	-1.0 \pm 0.2	-0.7\pm0.1	-1.5\pm0.1	WR111
4	3300	-0.1	-0.6\pm0.1	-1.2 \pm 0.2	< -0.7	< -1.5 C II 0.99 absent	WR143, BAT11
WO stars							
WO Subtype	C IV 1.74 μ m	log W λ (O VI 1.07/ C IV 1.19)	log W λ (He II 1.16/ C IV 1.19)	log W λ (O VI 1.46+He II 1.47)/ C IV 1.74)	log W λ (C IV-III 2.07-2.11/ (C IV 2.43 + O VI 2.46)	log W λ (C III 0.97/ He II 1.01) Notes	Templates
4	3600	-0.8	-0.7	-0.3	0.2	-0.7 O VI 1.075, 1.46, 2.46	LH41-1042
3	4200	-0.8	-0.7	-0.5	≤ 0.0	C III weak O VI 1.075, 1.46, 2.46	WR93b
2	6300	-0.8	≤ -1	-0.5	-1.0	C III absent O VI 1.075, 1.46, 2.46	WR102

Table 4. Near-IR equivalent width and FWHM measurements for newly identified Galactic WN stars plus previously discovered WN stars lacking optical spectroscopy. Equivalent widths (in Å) are generally robust to ± 0.05 dex, except for weak lines ± 0.1 dex, while measured FWHM (in km s^{-1}) are generally reliable to $\pm 50 \text{ km s}^{-1}$ (approximate values are indicated with colons). The key to the spectroscopic datasets utilised is provided in Table 2.

WR	WN	He II 1.01	He I 1.08	P γ	N v 1.11	He II 1.16	P β	He II 1.48	N v 1.55	He II 1.69	He I 1.70	He I 2.06	N III-v 2.11	Br γ	He II 2.19	Note	Data		
	SpType	FWHM	$\log W_\lambda$	$\log W_\lambda$	$\log W_\lambda$	$\log W_\lambda$	$\log W_\lambda$	$\log W_\lambda$	$\log W_\lambda$	$\log W_\lambda$	$\log W_\lambda$	$\log W_\lambda$	$\log W_\lambda$	$\log W_\lambda$	FWHM	$\log W_\lambda$			
WR47-5	WN6(h)	1000	1.82	1.90	1.1	1.76	1.59	1.54		0.95	<0.4		1.3:	1.58	1630	1.59	2.11>2.10	N6	
WR56-1	WN5o	1220	2.09	1.78		1.73	1.32	1.50		1.18	0.9:		1.45	1.30	1200	1.56	2.11>2.10	N6	
WR60-8	WN6o	1510	2.28	2.27	1.31	0.7:	2.10	1.72	1.82		1.53	1.26		1.46	1.63	1670	1.83	2.11>2.10	N6
WR62a	WN6o	1670	1.82	1.73	0.7:		1.55	1.09	1.30				1.18	1.28	1650	1.48	2.11>2.10	N2	
WR64-2	WN6o	1480	2.29	2.26	1.33		2.08	1.67	1.83		1.50	1.18		1.54	1.64	1640	1.97	2.11>2.10	N6
WR64-3	WN6o	1340	2.18	2.20	1.40		2.02	1.80	1.75		1.40	1.08		1.45	1.60	1710	1.79	2.11>2.10	N6
WR64-4	WN6o+	1930	1.87	2.00	1.04		1.71	1.43	1.48	0.5:	1.20	0.94		1.08	1.20	2220	1.56	2.11>>2.10	N6
WR64-5	WN6o	1680	2.09	2.25	1.18	0.8:	1.91	1.62	1.69	0.6:	1.30	1.20		1.48	1.54	1670	1.79	2.11>>2.10	N6
WR64-6	WN6b	2130	2.39	2.54	1.27		2.17	1.84	1.91	0.7	1.56	1.40		1.55	1.61	2300	1.99	2.11>>2.10	N6
WR68a	WN6o	1680	1.92	1.81	0.8	0.5:	1.68	1.31	1.46	0.6				1.30	1.41	1570	1.54	2.11>2.10	N2
WR70-14	WN4b	2760	2.49	2.33			2.38	1.95	2.11		1.65	1.3:		1.69	1.89	2800	2.23	2.11~2.10	N6
WR70-15	WN5o	1450:	2.3:	1.85	1.2:		2.17	1.67	1.90	0.6	1.58	<0.5		1.38	1.43	1740	1.98	2.11>2.10	N6
WR72-5	WN6o	1370	2.23	2.25	1.2		2.07	1.69	1.82	0.5	1.52	1.26	0.6:	1.63	1.66	1500	1.92	2.11>>2.10	N6
WR75-31	WN7o	1250:	1.7:	2.3:			1.95	1.78	1.67					1.72	1.71	1370	1.72	2.11~2.19	N6
WR75-30	WN7o										1.34	1.59	0.8:	1.84	1.79	1880	1.82	2.11~2.19	N6
WR76-11	WN7o										1.15	1.57	1.1	1.64	1.67	1260	1.59	2.11~2.19	N6
WR93a	WN6h	1800	1.91	1.85	1.71		1.71	1.98	1.38					1.38	1.88	1770:	1.59	2.11>2.10	N2

Note: 2.10 = N v 2.100; 2.11 = He I 2.112 + N III 2.116; 2.19 = He II 2.189

Table 5. Near-IR equivalent width and FWHM measurements for newly identified Galactic WC stars plus previously discovered WC stars lacking optical spectroscopy. Equivalent widths (in Å) are generally robust to ± 0.05 dex, except for weak lines ± 0.1 dex, while measured FWHM (in km s^{-1}) are generally reliable to $\pm 50 \text{ km s}^{-1}$. The key to the spectroscopic datasets utilised is provided in Table 2.

WR	WC	C III 0.97	C II 0.99	He II 1.01	He I 1.08	He II 1.16	C IV 1.19	C III 1.20	C IV 1.43	He I-II 1.70	C IV 1.74	C II 1.78	He I 2.06	C IV 2.07	C III 2.11	Data		
	SpType	$\log W_\lambda$	$\log W_\lambda$	FWHM	$\log W_\lambda$	$\log W_\lambda$	$\log W_\lambda$	$\log W_\lambda$	$\log W_\lambda$	$\log W_\lambda$	FWHM	$\log W_\lambda$	$\log W_\lambda$	$\log W_\lambda$	$\log W_\lambda$			
WR46-18	WC6-7	2.72	<1.1	3290	2.24	2.38	2.09	2.26	1.81	1.88	1.62	3040	2.33		3.02	2.36	N6	
WR60-7	WC7-8	2.99	1.63	1640	2.08	2.36	2.05	2.25	1.89	2.25	1.56	1770	2.26		2.89	2.34	N6	
WR70-13	WC8d	2.89	1.68	1350	1.72	2.34	1.85	1.94	2.01	2.01	1.54	1300	1.90	1.84	2.31	2.03	N6	
WR75aa	WC9d	2.72	1.67	1060	1.41	2.26	1.76	1.75	1.98	1.75	1.11	1330	1.30	1.54	1.64	1.57	N5	
WR75c	WC9	2.58	1.70	990	1.30	2.63	1.69	1.60	2.12	1.82	1.81	1190	1.58	2.14	2.43	2.00	2.16	N5
WR107a	WC5-7	3.11	1.72	2170	2.24	2.25	2.12	2.47	1.83	2.34					2.94	2.25	N2	

5 NEW GALACTIC WOLF-RAYET STARS

We have identified 16 new Wolf-Rayet stars, which we have assigned Galactic WR numbers, in accordance with the current IAU convention (see Appendix of RC15). Here we discuss their spectral types, spatial location and their potential association with Scutum-Crux or other spiral arms. Near-IR spectra of the new WR stars are presented in Figures 2 (IJ) and 3 (HK), together with our NTT/SOFI observations of WR75aa, WR75c, the recently discovered WN star WR75-30 (Kanarek et al. 2015), plus previously unpublished NTT/SOFI spectroscopy of WR62a, WR68a, WR93a, WR107a, as discussed above. Line measurements are provided in Table 4 and 5 for WN and WC stars, respectively, with diagnostic line ratios presented in Table 6.

5.1 Classification of the new WR stars

5.1.1 Broad-lined WN stars

Only two of the new WN stars, WR64–6 and WR70–14, are identified as broad-lined WN stars, owing to their He I $1.01\mu\text{m}$ line widths ($\text{FWHM} > 1900 \text{ km s}^{-1}$) and strengths ($\log W_\lambda/\text{\AA} \geq 2.4$), albeit WR64-6 only narrowly complies with the second criterion. A WN6b subtype is favoured for WR64–6 from its He I 1.08/He II 1.01 μm ratio which is supported by $(\text{N III} + \text{He I } 2.11) > \text{N v } 2.10$, while both hydrogen criteria (involving $\text{P}\beta$ and $\text{Br}\gamma$) indicate no hydrogen, so we adopt WN6b for this star. For WR70–14, the He I 1.08/He II 1.01 μm ratio is somewhat ambiguous, consistent with WN4–6b, but $(\text{N III} + \text{He I } 2.11) \sim \text{N v } 2.10$ favours WN4b. This is supported by weak N v 1.11 μm in the J-band (Fig. 2). Again, there is no evidence for atmospheric hydrogen from our criteria (Fig. A4, available online), so WN4b is assigned to WR70–14.

5.1.2 Narrow-lined WN stars

The remaining 11 WN stars are a relatively homogeneous group, almost all classified as either WN5o, WN6o or WN7o stars, with only WR47–5 showing evidence of hydrogen so we consider these according to their subtype.

The two highest ionization narrow-lined stars are WR56-1 and WR70-15, according to their He I 1.08/He II 1.01 ratios (Fig. A3, available online), which indicate WN5 for both stars. This is supported by the He I 1.70/He II 1.69 ratio for WR56-1, although an earlier WN3–4 subtype is favoured by He I 1.70/He II 1.69 for WR70-15. We also consider their K-band morphologies, for which $(\text{N III} + \text{He I } 2.11) > \text{N v } 2.10$ in both cases, indicating WN5–6. Neither star shows any evidence for atmospheric hydrogen from Fig. A4 so we adopt WN5o for both stars.

The majority of our narrow-lined WN stars are WN6 stars according to their He I 1.08/He II 1.01 ratios (Fig. A3), with He I 1.70/He II 1.69 suggesting WN4, 5 or 6. As with the WN5o stars considered above, we also consider the K-band morphology, for which either $(\text{N III} + \text{He I } 2.11) > \text{N v } 2.10$, implying WN5–6 or $(\text{N III} + \text{He I } 2.11) \gg \text{N v } 2.10$, implying WN6. Only WR47–5 indicates the presence of (modest) hydrogen from Fig. A4, such that we classify it as WN6(h), but favour WN6o for WR60-8, WR64-2, -3, -4, -5 and WR72-5.

Of the remaining stars only WR75-31 was observed in

the IJ-band with SOFI, for which He I 1.08/He II 1.01 indicates a WN7–8 subtype, with He I 1.70/He II 1.69 also providing an ambiguous WN7–8 classification. Its K-band morphology strongly favours WN7 since $(\text{N III} + \text{He I } 2.11) \sim \text{He II } 2.19$, while there is no evidence for atmospheric hydrogen in WR75-31 from Fig. A4, such that we assign WN7o to this star. WR76-11 was observed solely in the H and K bands, but closely resembles WR75-31 such that we classify it as WN7o, as with WR75-30. None of the new WN stars qualify as WN/C stars, since C III 0.971 μm , C IV 1.19 μm , 1.74 μm , 2.07 μm are weak/absent.

5.1.3 WC stars

Three of the new WR stars are carbon sequence WC stars. Considering the primary diagnostics for WR46–16, WC7 is favoured from the C IV 1.19/C III 1.20 ratio, WC4–6 from the C III 0.97/C II 0.99 ratio, and WC5–7 from the C IV 2.07/C III 2.11 ratio. Secondary indicators suggest WC5–7 from He I 1.08/He II 1.01, WC5–6 from C III 0.97/He II 1.01 and WC6–7 from He I-II 1.7/C IV 1.74. Overall, we adopt WC6–7 reflecting the tension in primary indicators for WR46–16 (Fig. A7, available online).

WR60–7 is classified as WC8, WC7, WC7–8 from primary diagnostics C IV 1.19/C III 1.20, C IV 2.07/C III 2.11 and C III 0.97/C II 0.99, respectively. Secondary criteria C III 0.97/He II 1.01 and He I-II 1.7/C IV 1.74 indicate WC6–7, while He I 1.08/He II 1.01 favours WC7–8. Overall, WC7–8 is selected for WR60–7, reflecting the lack of a consensus amongst primary criteria (Fig. A7).

Finally, primary diagnostics C IV 1.19/C III 1.20, C IV 2.07/C III 2.11 and C III 0.97/C II 0.99, imply WC8–9, WC8 and WC8–9 for WR70–13, while C IV 1.74 \geq C II 1.78 indicates WC8. Consequently we adopt WC8 for WR70–13, which is supported by our secondary indicator He I-II 1.7/C IV 1.74, with He I 1.08/He II 1.01 and C III 0.97/He II 1.01 consistent with either WC8 or WC9 (Fig. A7).

5.2 Binarity

Approximately 40% of the Galactic WR population are observed in multiple systems (van der Hucht 2001). This is a lower limit on the true binary fraction, since no systematic survey has been carried out. It is therefore highly likely that some of the newly discovered WR stars are in fact multiple systems. Direct detection of companion stars, usually main-sequence OB stars, is not possible with the current dataset since their absorption lines are generally weak with respect to the strong WR emission lines.

It is, however, possible to infer the presence of a companion star by considering the equivalent width of near-IR emission lines which will be diluted by the continuum of a companion star, and/or dust for the case of some WC+OB systems since dust formation is an indicator of binarity in WC stars.

Since a companion star and/or thermal dust emission will not reduce line widths, a weak line compared to single stars at a specific FWHM is suggestive of binarity. In Figure 4 we compare the FWHM (km s^{-1}) and equivalent widths (in \AA) of strong, isolated lines in apparently single Galactic WN stars (He II 1.012 μm) and WC stars (C IV

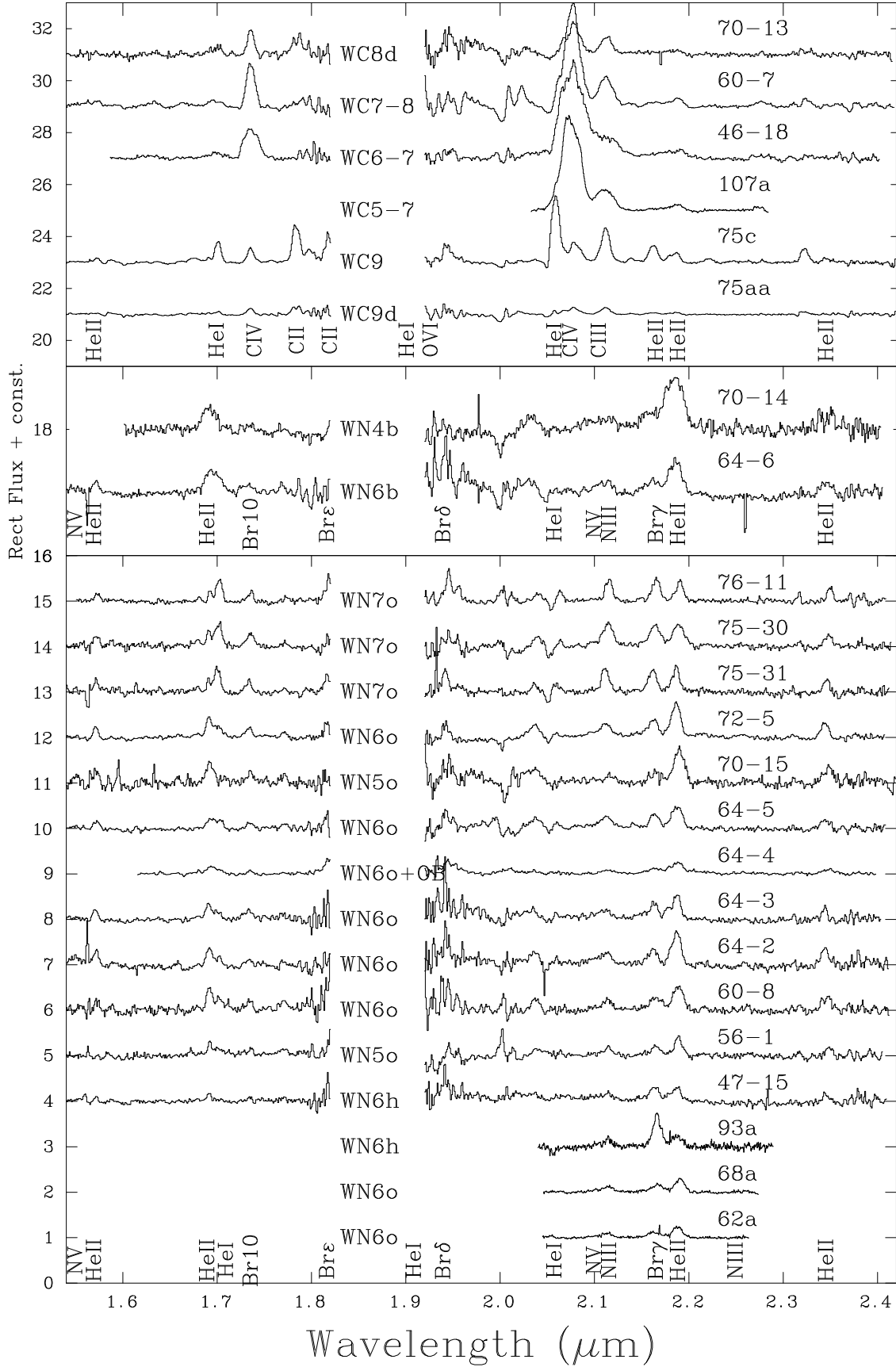


Figure 3. HK-band spectra of new WR stars, plus unpublished NTT/SOFI spectroscopy of previously identified WR stars (WR62a, WR68a, WR75aa, WR75c, WR93a and WR107a) plus our NTT/SOFI spectroscopy of WR75–30.

Table 6. Ratios of near-IR diagnostic lines for newly identified Wolf-Rayet stars from NTT/SOFI spectroscopy plus revised near-IR classifications for previously known stars. Line strengths/widths are provided for He II 1.012 μ m (2.189 μ m in parenthesis) or C IV 1.736 μ m (1.190 μ m in parenthesis) for WN and WC stars, respectively.

ID	WR	1.01 μ m FWHM km s ⁻¹	log W_λ (He I 1.08/ He II 1.01)	log W_λ (P β / He II 1.16)	log W_λ (He I 1.70/ He II 1.69)	log W_λ (Br γ / He II 2.19)	log W_λ (He I+N III 2.11/ N V 2.10)	Old SpT	Ref	New SpT			
B#13	WR47-5	1000	+0.08	WN6	-0.17 (h)	-0.55	WN4	-0.01 (h)	>0	WN5-6	-	-	WN6(h)
B#37	WR56-1	1220	-0.31	WN5	-0.41 o	-0.28	WN5	-0.26 o	>0	WN5-6	-	-	WN5o
B#56	WR60-8	1510	-0.01	WN6	-0.38 o	-0.27	WN5	-0.20 o	>0	WN5-6	-	-	WN6o
	WR62a	1670	-0.09	WN6	-0.46 o	—	—	-0.20 o/(h)	>0	WN5-6	WN5o	S99	WN6o
B#85	WR64-2	1480	-0.03	WN6	-0.41 o	-0.32	WN5	-0.33 o	>0	WN5-6	-	-	WN6o
B#87	WR64-3	1340	+0.02	WN6	-0.22 o/(h)	-0.32	WN5	-0.19 o	>0	WN5-6	-	-	WN6o
B#88	WR64-4	1930	+0.13	WN6	-0.28 o	-0.26	WN5	-0.36 o	\gg 0	WN6	-	-	WN6o+OB
B#91	WR64-5	1680	+0.16	WN6	-0.29 o	-0.10	WN6	-0.25 o	\gg 0	WN6	-	-	WN6o
B#93	WR64-6	2130	+0.15	WN6b	-0.33 o	-0.16	WN6b	-0.38 o	>0	WN6b	-	-	WN6b
	WR68a	1680	-0.11	WN6	-0.37 o	—	—	-0.13 o/(h)	>0	WN5-6	WN6o	S99	WN6o
B#107	WR70-14	2760	-0.16	WN4-6b	-0.43 o	-0.35	WN6b	-0.34 o	\approx 0	WN4b	-	-	WN4b
B#123	WR70-15	1450	-0.45	WN4-5	-0.50 o	-1.08	WN2-4	-0.55 o	>0	WN5-6	-	-	WN5o
B#132	WR72-5	1370	+0.02	WN6	-0.38 o	-0.26	WN5:	-0.26 o	\gg 0	WN6	-	-	WN6o
A#11	WR75-31	1250	+0.60:	WN7-8	-0.17 o	+0.39	WN7-8	-0.01 o	0.00 \ddagger	WN7	-	-	WN7o
A#13	WR75-30	(1880)	—	—	—	+0.25	WN7	-0.03 o	0.02 \ddagger	WN7	WN6	K15	WN7o
B#154	WR76-11	(1260)	—	—	—	+0.42	WN7-8	-0.08 o	0.05 \ddagger	WN7	-	-	WN7o
	WR93a	1800	-0.06	WN6	+0.27 h	—	—	+0.29 h	\gg 0	WN6	WN6	M13	WN6h

ID	WR	1.74 μ m FWHM km s ⁻¹	log W_λ (He I 1.08/ He II 1.01)	log W_λ (C III 1.20/ C IV 1.19)	log W_λ (He I-II 1.70/ C IV 1.74)	log W_λ (C III 2.11/ C IV 2.07)	log W_λ (C II 0.99/ C III 0.97)	Old SpT	Ref	New SpT					
E#3	WR46-18	3100	+0.14	WC6-7	-0.45	WC7	-0.71	WC6-7	-0.66	WC4-7	-1.62	WC4-6	-	-	WC6-7
B#51	WR60-7	1800	+0.28	WC7-8	-0.36	WC8	-0.70	WC6-7	-0.55	WC7-8	-1.36	WC7-8	-	-	WC7-8
B#105	WR70-13	1300	+0.62	WC8-9	+0.07	WC8-9	-0.36	WC8	-0.28	WC8	-1.21	WC8-9	-	-	WC8d
	WR75aa	1400	+0.85	WC9	+0.23	WC9	-0.19	WC8-9	-0.07	WC9	-1.05	WC9	WC9d	H05	WC9
	WR75c	1350	+1.33	WC9	+0.52	WC9	+0.23	WC9	+0.19	WC9	-0.88	WC9	WC9	H05	WC9
	WR107a	(2400)	+0.01	WC5	-0.64	WC5-7	—	-0.69	WC5-7	-1.39	WC5-8	WC6	S99	WC5-7	

S99 (Shara et al. 1999), H05 (Hopewell et al. 2005), M13 (Miszalski et al. 2013), K15 (Kanarek et al. 2015)

\ddagger : log W_λ (He I 2.112 + N III 2.116/He II 2.189)

1.736 μ m) with newly discovered WR stars. We also include weak-lined WN stars with intrinsic absorption lines (WR24, WR87, WR108) which could be mistaken for WN+OB stars, plus dusty WC stars (WR121, WR75aa), whose near-IR emission lines are diluted by hot dust.

Of the newly identified stars, the majority of WR stars possess emission line strengths which are characteristic of single stars. From Fig. 4(a) two exceptions are WR75-31 (WN7(h)) and WR64-4 (WN6o) which possess weak emission for their He II 1.012 μ m FWHM. Both are potential binaries, although WR64-4 is the strongest candidate, such that we revise its spectral type to WN6o+OB. In contrast, WR75-31 has an overall relatively strong emission line spectrum, albeit with an anomalously weak (and low S/N) He II 1.0124 μ m line.

Of the WC stars, none possess unusually weak emission lines based on their C IV 1.736 μ m FWHM (Fig. 4(b)). However, the increased dilution of WC emission lines from 1 μ m to 2.5 μ m arising from hot dust in WCd systems also severely modifies equivalent width ratios of C III-IV lines. For example, $W_\lambda(\text{C III } 2.11)/W_\lambda(\text{C III } 0.97) = 0.3$ for WR88 (WC9) but hot dust in WR121 (WC9d) reduces this ratio to 0.05. A similar reduction in line strength is observed for promi-

nent He II lines, with $W_\lambda(\text{He II } 2.19)/W_\lambda(\text{He II } 1.28) = 0.5$ for WR88 and 0.17 for WR121. WR135 is a prototypical non-dusty WC8 star with $W_\lambda(\text{C III } 2.11)/W_\lambda(\text{C III } 0.97) = 0.2$, with a ratio of 0.2 for WR60-7 but only 0.1 for WR70-13, suggestive of dust dilution in the latter. Indeed, WR60-7 (WC7-8) and WR70-13 (WC8) possess similar J-H colours, yet the latter has 0.5 mag higher $K_S-[8]$ colour (Table 1), so we amend its spectral type to WC8d. Indeed, WR70-13 is offset from the other WC stars in the reddening free Q1 vs Q2 comparison in Fig. 1. Turning to WR46-18, $W_\lambda(\text{C III } 2.11)/W_\lambda(\text{C III } 0.97) \sim 0.3$ for non-dusty WC6-7 stars, with a ratio of 0.4 for WR46-18, arguing against dust emission in this instance.

Discovery of a hard X-ray source associated with any of the WR stars would be highly indicative of stellar wind collision in a massive binary. Indeed, several WR stars towards the Galactic Centre, coincide with hard X-ray sources (e.g., Mauerhan et al. 2010, Nebot Gómez-Morán et al. 2015). From a search of the XMM Newton science archive and the Chandra source catalogue (1.0), fields including WR60-7 (WC7-8), WR60-8 (WN6o), and WR64-4 (WN6o) had been imaged by Chandra ACIS, although none revealed a source at the location of the WR star.

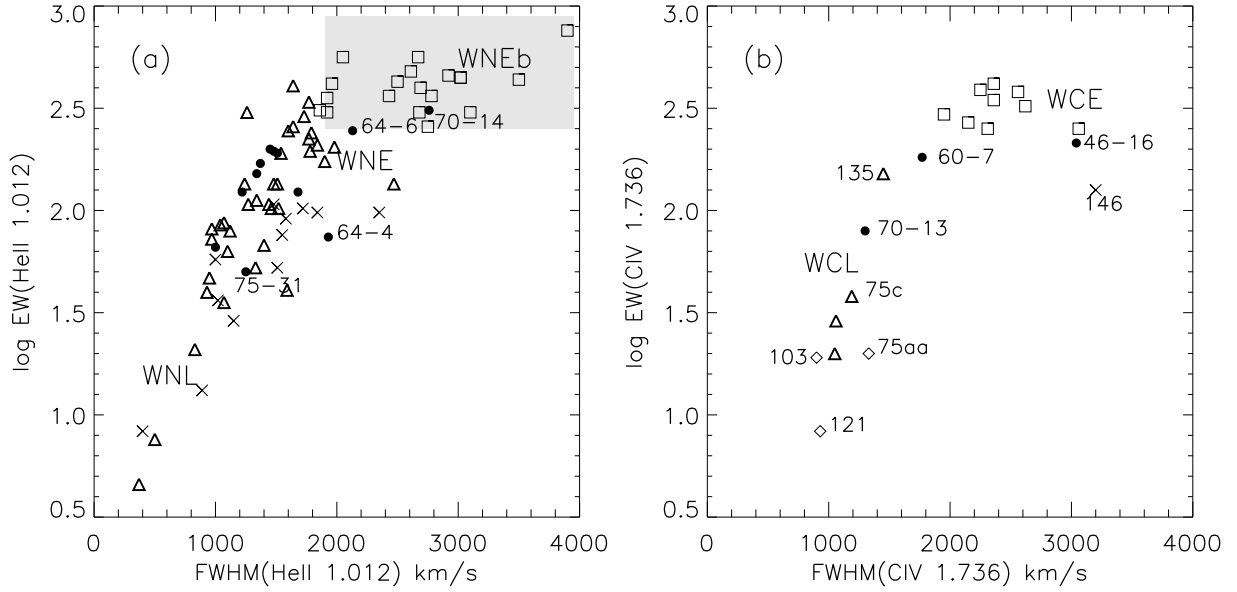


Figure 4. (a): FWHM (in km s^{-1}) vs equivalent width (in \AA) for $\text{He II } 1.012\mu\text{m}$ in apparently single Galactic broad-lined WN stars (open squares), weak-lined WN stars (open triangles) and WNha/+abs stars (crosses) together with the newly identified WN stars (filled circles). The grey region indicates the parameter space covered by broad-lined WN stars. (b): FWHM (in km s^{-1}) vs equivalent width (in \AA) for $\text{C IV } 1.74\mu\text{m}$ in apparently single Galactic WC4–7 stars (open squares), WC8–9 stars (open triangles) plus WCd/WC+O systems (crosses) together with the newly identified WC stars (filled circles).

5.3 Spatial location of the new WR stars

We have estimated distances to the new WR stars by adopting an absolute K_S -band magnitude based on the assigned spectral subtype. To do this, we followed the approach of RC15, which we briefly summarise here. To calculate the foreground dust extinction to each new WR star, we used subtype-specific intrinsic J–H and H– K_S colours to measure a colour excess. Using the near-IR extinction law of Stead & Hoare (2009), we thereby obtained two measures of extinction in the K_S -band, of which an average was taken. Distances were then calculated using the standard relation between absolute and apparent magnitude. We used the uncertainties on calibrated absolute magnitudes, given by RC15, to calculate upper and lower bounds on the distances calculated. In Table 7 we provide interstellar extinctions, distance moduli/distances, with uncertainties, for every new WR star. Typical extinctions are $A_K = 1.2 \pm 0.2$ mag, with characteristic distances of 9.7 ± 3.8 kpc.

This method inherently assumes the WR star is the sole (or dominant) contributor of near-IR flux to each source. Recalling Sect. 5.2, this assumption is justified for new WN stars with the exception of WR64-4, the emission line strengths of which suggest a significant contribution from a companion source, implying a larger distance. In addition, we provide a second distance estimate to WR70-13 in Table 7 since there is evidence for a contribution by circumstellar dust to the K-band. Adopting the absolute magnitude of a WC8 star which is dominated by hot dust would significantly increase the distance to WR70-13 from 5.3 to 10.7 kpc, though in reality the dust contribution is likely to be modest such that an intermediate distance is more realistic.

5.4 Association of WR stars with the Scutum-Crux and other spiral arms

In Figure 5 we present the locations of the new WR stars on a top-down view of the Galactic disk, together with WR stars mapped by RC15 (including approximately half of the currently known population). Over-plotted are the locations of the three main spiral features detected in the 4th Galactic quadrant ($270 < l < 360$), assuming $R_G = 8.0$ kpc. We assume each arm is a logarithmic spiral, parameterised as:

$$x = r \cos(\theta), \quad y = r \sin(\theta), \quad r = r_t \exp[(\theta - \theta_0) \tan(p)]. \quad (1)$$

in which r_t is the Galactocentric radius of the observed tangent, θ is the angle measured anti-clockwise about the origin from the positive x-axis, and θ_t is the angle at which the observed tangent is located. The parameter p is the pitch angle of the arm. The calculation of r_t requires a measurement of the longitude of the tangent to each arm (l_t), and the Galactocentric radius of the Sun (R_G).

$$r_t = R_G \sin(360^\circ - l_t) / \sin(90^\circ - p). \quad (2)$$

Vallée (2014) catalogued the observed tangents to spiral arms in the Galaxy, and calculate averages of measurements using different tracers. Subsequently, Vallée (2015) use these observations to measure pitch angles for individual spiral arms. From these studies we adopt $l_t = 284^\circ$ & $p = 14^\circ$ for the Sagittarius-Carina arm, 310° & 13.3° for the Scutum-Crux arm, and 328° & 9.9° for the Norma (3kpc) arm.

The new WR stars appear to be evenly distributed throughout the section of Galactic disk observed; neither they, nor the previously mapped WR stars, show any obvious association to the spiral features in the region. Indeed, no pattern resembling a spiral arm can be seen in the dis-

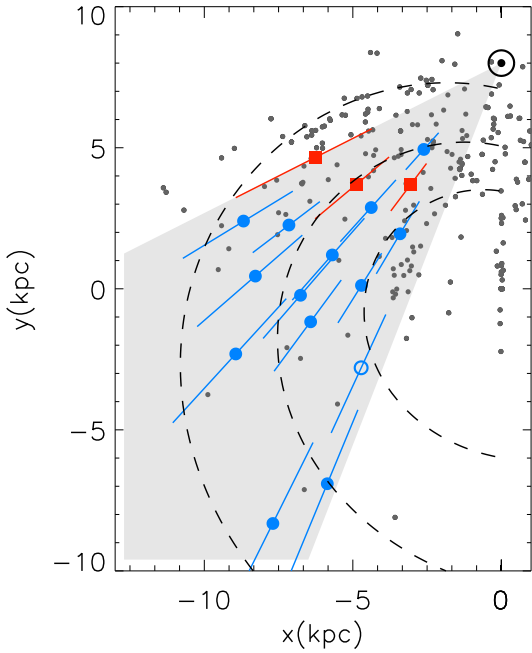


Figure 5. A top-down view of the Galactic disk showing the 4th quadrant. The x-axis is parallel to the line-of-sight in the direction $l = 270^\circ$. Shaded grey is the swathe of Galactic longitude constituting the survey area ($298^\circ < l < 340^\circ$). New WN stars are shown as filled blue circles (WR75-30 is an open symbol), new WC stars are shown as filled red squares, while 355 previously identified WR stars are small grey circles (Rosslowe & Crowther 2015a). Dashed lines show the measured locations of prominent spiral arms in this Galactic quadrant, represented as logarithmic spirals.

tribution of WR stars, as would be expected if they were tightly confined to spiral arms, albeit affected by a systematic offset in distance measurements. The upcoming second data release (DR2) from *Gaia* should address this general question, although the majority of the newly discovered WR stars are too faint for reliable parallaxes with *Gaia*. Indeed, only 7 of the 17 stars are included in the *Gaia* first data release (DR1 Gaia Collaboration et al. 2016), with $G = 17.4 - 20.1$ mag.

6 SPATIAL DISTRIBUTION OF WOLF-RAYET STARS AND OTHER MASSIVE STARS IN THE MILKY WAY

6.1 Association of WR stars with star clusters?

If the majority of WR progenitors are born in relatively massive star-forming regions, one might expect them to be in close proximity to their natal star cluster. We have compared the spatial location of the new WR stars with young star clusters from Dutra et al. (2003), Mercer et al. (2005) and Borissova et al. (2011). None of the new WR stars are located within known clusters. At face value, this might be considered to be surprising, but Lundstrom & Stenholm (1984) in the most extensive study of the environment of

Table 7. Estimated interstellar extinctions and distances to the newly discovered WR stars, following the methodology of C15. Two entries are provided for the WR70-13, the second appropriate for a dusty WC8 star. We also provide a distance estimate to the recently identified star WR75-30 (Kanarek et al. 2015) resulting from our new spectroscopic classification.

WR	Spec. Type	M_{K_S} mag	A_{K_S} mag	DM mag	d kpc
WR46-18	WC6-7	-4.75 ± 0.77	0.97 ± 0.10	14.25 ± 0.78	$7.1^{+3.0}_{-2.1}$
WR47-5	WN6(h)	-4.94 ± 0.46	0.96 ± 0.02	15.07 ± 0.46	$10.3^{+2.4}_{-2.0}$
WR56-1	WN5o	-3.86 ± 0.34	1.23 ± 0.00	14.81 ± 0.34	$9.2^{+1.6}_{-1.3}$
WR60-7	WC7-8	-4.94 ± 0.55	1.16 ± 0.02	14.06 ± 0.55	$6.5^{+1.9}_{-1.3}$
WR60-8	WN6o	-4.94 ± 0.46	1.45 ± 0.05	15.25 ± 0.46	$11.2^{+2.6}_{-2.1}$
WR64-2	WN6o	-4.94 ± 0.46	1.15 ± 0.02	15.68 ± 0.46	$13.7^{+3.2}_{-2.6}$
WR64-3	WN6o	-4.94 ± 0.46	0.98 ± 0.01	14.14 ± 0.46	$6.7^{+1.6}_{-1.3}$
WR64-4	WN6o+	-4.94 ± 0.46	1.02 ± 0.04	13.02 ± 0.46	$4.0^{+0.9}_{-0.8}$
WR64-5	WN6o	-4.94 ± 0.46	1.00 ± 0.01	14.74 ± 0.46	$8.9^{+2.1}_{-1.7}$
WR64-6	WN6b	-5.16 ± 0.37	1.13 ± 0.01	15.14 ± 0.37	$10.7^{+2.0}_{-1.7}$
WR70-13	WC8d	-5.04 ± 0.41	1.38 ± 0.08	13.62 ± 0.42	$5.3^{+1.1}_{-0.9}$
		-6.57 ± 0.41	1.38 ± 0.08	15.15 ± 0.42	$10.7^{+2.3}_{-1.9}$
WR70-14	WN4b	-4.85 ± 0.38	1.11 ± 0.04	15.24 ± 0.38	$11.2^{+2.1}_{-1.8}$
WR70-15	WN5o	-3.86 ± 0.34	1.45 ± 0.01	14.81 ± 0.34	$9.2^{+1.6}_{-1.3}$
WR72-5	WN6o	-4.94 ± 0.46	1.00 ± 0.00	14.21 ± 0.46	$6.9^{+1.6}_{-1.3}$
WR75-31	WN7o	-5.49 ± 0.42	1.42 ± 0.02	16.28 ± 0.42	$18.0^{+3.9}_{-3.2}$
WR75-30	WN7o	-5.49 ± 0.42	1.70 ± 0.06	15.36 ± 0.42	$11.8^{+2.5}_{-2.1}$
WR76-11	WN7o	-5.49 ± 0.42	1.45 ± 0.05	16.02 ± 0.42	$16.0^{+3.4}_{-2.8}$

Galactic WR stars to date, found that only 10–30% of WR stars are located in star clusters.

Since then, the known WR population has quadrupled, so we provide revised statistics for the $298^\circ \leq l \leq 340^\circ$ survey region as a whole, involving 190 + 16 = 206 Galactic Wolf-Rayet stars, comprising 119 WN, 1 WN/C and 86 WC stars. Lundstrom & Stenholm (1984) considered a WR star to be associated with a star cluster if its projected distance was within two cluster radii. Here, we soften this requirement, extending the potential association to 4 cluster radii, utilising published cluster centres and radii from Dias et al. (2002), Dutra et al. (2003), Mercer et al. (2005), Borissova et al. (2011). Overall, 55 WR stars (27%) are associated with a total of 12 star clusters, as shown in Table 8, although it is notable that 44% of all the WR cluster members in our survey range are located within a single open cluster, Westerlund 1 (C06). Consequently 73% of WR stars in the survey region are *not* associated with a star cluster.

If the majority of WR progenitors are born in relatively massive star forming regions, why are so few currently associated with clusters? The lower WR mass limit for single rotating stars at Solar metallicity is $\sim 22 M_\odot$ star (Meynet & Maeder 2003). Empirically, such stars are observed in clusters with $\geq 500 M_\odot$ (Larson 2003; Weidner et al. 2010). Stochasticity in the sampling of the initial mass function will result in some massive stars originating in low mass ($10^2 M_\odot$) clusters/star-forming regions, as demonstrated theoretically by Parker & Goodwin (2007). Therefore, some WR stars could be associated with low mass clusters, with other members of the star forming region inconspicuous. Indeed, γ Vel (WC8+O), the closest Galactic

Table 8. Galactic WR stars hosted by a star cluster in the range $298^\circ \leq l \leq 340^\circ$, updated from [Lundstrom & Stenholm \(1984\)](#). We consider WR stars to be associated with a cluster if $r \leq 4R$, representing 27% of the known WR content of this region of the Milky Way.

Cluster	Alias	l deg	b deg	d kpc	R arcmin	Ref	WN (r , arcmin)	WC (r , arcmin)	Ref
	VVV CL 011	298.506	-0.170	5.0:	0.1	d, l	WR46-17 (0.0)		d
	Mercer 30	298.756	-0.408	7.2	0.3	a, j	WR46-3 (0.2), WR46-4 (0.1) WR46-5 (0.1), WR46-6 (0.2)		a a
C 1240-628	Hogg 15	302.047	-0.242	3.0	3.5	k	WR47 (1.6)		b
C 1309-624	Danks 1	305.339	+0.080	4.2	0.75	c, k	WR48-8 (0.6), WR48-9 (0.6) WR48-10 (0.6), WR48-6 (2.7) WR48-7 (2.5)	WR48a (1.3), WR48-3 (1.9) WR48-4 (2.4)	c c c
C 1310-624	Danks 2	305.393	+0.088	4.2	0.75	c, k		WR48-2 (0.6)	c
	VVV CL 036	312.124	+0.212	2.0:	0.8	d, l	WR60-6 (0.1)		d
	VVV CL 041	317.109	+0.281	4.2	0.5	e, l	WR62-2 (0.2)		e
	Pismis 20	320.516	-1.200	3.6	2.0	k	WR67 (2.1)		i
	Mercer 70	329.697	+0.584	7.0	0.4	f, j		WR70-12 (0.4)	f
	VVV CL 073	335.894	+0.133	4.0:	0.3	d, l	WR75-25 (0.1), WR75-26 (0.1)		d
	VVV CL 074	336.373	+0.194	6.0:	0.55	d, l	WR75-28 (0.1), WR75-29 (0.0)	WR75-27 (0.3)	d
	Mercer 81	338.384	+0.111	11.0	0.6	g, j	WR76-2 (0.6), WR76-3 (0.7) WR76-4 (0.9), WR76-5 (0.8) WR76-6 (0.9), WR76-7 (0.9) WR76-8 (0.9), WR76-9 (1.0)		g g g g
C 1644-457	Westerlund 1	339.555	-0.399	3.8	1.2	m, n, k	WR77a (1.7), WR77c (0.8) WR77d (1.1), WR77e (0.4) WR77f (0.4), WR77h (0.1) WR77j (0.7), WR77k (0.4) WR77o (0.4), WR77q (0.5) WR77r (0.8), WR77s (0.5) WR77sa (0.4), WR77sb (2.0) WR77sc (0.8), WR77sd (2.8)	WR77aa (4.1), WR77b (4.8) WR77g (0.1), WR77i (0.9) WR77l (0.6), WR77m (0.4) WR77n (1.7), WR77p (0.8)	h h h h h h h h

a: [Kurtev et al. \(2007\)](#); b: [Sagar et al. \(2001\)](#); c: [Davies et al. \(2012b\)](#); d: [Chené et al. \(2013\)](#); e: [Chené et al. \(2015\)](#); f: [de la Fuente et al. \(2015\)](#); g: [Davies et al. \(2012a\)](#); h: [Crowther et al. \(2006\)](#) i: [Lundstrom & Stenholm \(1984\)](#) j: [Mercer et al. \(2005\)](#) k: [Dias et al. \(2002\)](#) l: [Borissova et al. \(2011\)](#) m: [Kothes & Dougherty \(2007\)](#) n: [Koumpia & Bonanos \(2012\)](#)

WR star, is located in a very low mass star-forming region ([Jeffries et al. 2014](#)). Other members of such star-forming region would be very difficult to identify at the typical distance of Galactic WR stars.

There is evidence that some dense, young massive clusters rapidly achieve virial equilibrium (e.g. [Hénault-Brunet et al. 2012](#)), such that they would retain the bulk of their stellar content over the representative WR ages of 5–10 Myr ([Meynet & Maeder 2003](#)). Indeed, the bulk of the WR stars associated with Westerlund 1 lie within the 1.2 arcmin radius – corresponding to 1.4 pc at a distance of 3.8 kpc – such that our 4 cluster radius limit is equivalent to ~ 5.5 pc. Of course not all open clusters are dense or bound. For example, Hogg 15 is a sparsely populated cluster with a much larger radius of 3 pc, at its distance of 3 kpc, so will be in the process of dispersing. Consequently the general lack of an association with star clusters is not wholly unsurprising. Indeed, inspection of the Galactic O Star Catalogue (GOSC v3.0 [Maíz Apellániz et al. 2013](#)) reveals 50 (optically visible) O stars in our survey region. Of these, only 18 (36%) are associated with a star cluster, not significantly larger than WR stars since the bulk of these are late-type O stars with comparable ages to many WR stars.

Of course, not all massive stars originate from star clusters. [Bressert et al. \(2010\)](#) demonstrated that only a small

fraction of star formation in the Solar Neighbourhood originates from dense environments. It is probable that the majority of OB stars originate from intermediate density regions, i.e. OB associations and/or extended star-forming regions (see [Parker & Dale 2017](#)). Indeed, [Wright et al. \(2016\)](#) have unambiguously demonstrated that the distributed massive stars in Cyg OB2 did not originate from a dense star cluster.

[Lundstrom & Stenholm \(1984\)](#) found that $\geq 50\%$ of optically visible WR stars were located in OB associations. It is not possible to calculate the fraction of IR-selected WR stars that lie within OB associations since the latter are limited to nearby optical surveys. Instead, it is necessary to compare the location of Wolf-Rayet stars with infrared catalogues of star-forming regions. We have compared the locations of all 206 WR stars in our survey region with confirmed H II regions from the all-sky WISE catalogue of Galactic H II regions from [Anderson et al. \(2014\)](#). In total, 53 stars are located within $\approx 1.5 R_{\text{HII}}$ of the H II region, representing 26% of the total WR population, as shown in Table 9. Of course, a subset of these WR stars will be foreground sources, so the quoted statistics represent strict upper limits.

The majority of these WR stars are associated with complexes at G298 (Dragonfish nebula), G305 and G338. By way of example, as many as twelve WR stars are associated

Table 9. Galactic WR stars coincident with star-forming regions in the range $298^\circ \leq l \leq 340^\circ$. We consider a WR star to be associated with a star-forming region (Anderson et al. 2014, WISE v1.4) if $r \leq 1.5R_{\text{HII}}$, although some WR stars will doubtless be foreground sources, such that 53/206 (= 26%) WR stars associated with star-forming regions represents a strict upper limit.

WISE H II	d kpc	R_{HII} arcmin	Ref	Cluster?	WN (r , arcmin)	WC (r , arcmin)	Ref
G298.224–0.334	11.1	5.0	a			WR46-7 (5), WR46-18 (8)	b, p
G298.529–0.251	10.5	16.2	a	VVV CL 011	WR46-8 (15.6), WR46-9 (3.5), WR46-17 (4.9)	WR46-10 (7.6)	b, c, d, e
					WR46-15 (16.9), WR46-2 (22.4)		g
G298.862–0.432	10.7	4.8	a	Mercer 30	WR46-3 (6.6), WR46-4 (6.6), WR46-5 (6.6), WR46-6 (6.6)		f
					WR47b (4.0)		f
G302.503–0.762	12.1	4.2	a		WR47-1 (18.9)		h
G302.631+0.030	4.6	14.3	a				e
G303.445–0.745	12.5	7.2	a			WR47-2 (2.6)	d
G305.233+0.110	4.9	11.3	a	Danks 1/2	WR48-6 (5.5), WR48-10 (6.5), WR48-7 (7.7) WR48-9 (6.8), WR48-8 (6.8)	WR48-1 (8.6), WR48-3 (6.0) WR48-4 (8.2), WR48a (8.4) WR48-2 (10.3)	e, g, h, i h, i
					WR48-5 (4.7)		b
G305.322–0.255	4.9	13.4	a		WR60-6 (7.8)		h
G311.991+0.219		6.0	a	VVV CL 036			c
G317.030+0.028*		24.4	a	VVV CL 041	WR62-2 (15.7), WR62-1 (19.4), WR63 (34)		h, j
G321.015–0.527	4.1	4.0	a		WR67-3 (6.1)		k
G321.115–0.546	3.8	4.2	a		WR67-1 (1.8)		l
G326.474–0.292		20.9	a			WR70-5 (17)	m
G327.824+0.117	7.2	3.9	a		WR70-6 (5.2)		g
G331.020–0.143		3.8	a			WR72-4 (3.5)	n
G335.794+0.153		13.7	a	VVV CL 073	WR75-6 (19.7), WR75-25 (6.1), WR75-26 (6.1)	WR75b (16.1), WR75-15 (12.4) WR75-16 (4.2)	h n
G336.446–0.198		10.4	a			WR75-9 (11.7), WR75-21 (10.3) WR75-5 (14.3) WR76-10 (4.7)	n d n
G338.350+0.221		6.9	a				n
G338.430+0.048		5.8	a	Mercer 81	WR76-2 (3.5), WR76-3 (3.5), WR76-4 (3.5) WR76-5 (3.5), WR76-6 (3.5), WR76-7 (3.5) WR76-8 (3.5), WR76-9 (3.5)		o o o
G338.911+0.615	4.4	3.8	a			WR76 (1.9)	o h

a: Anderson et al. (2014) b: Mauerhan et al. (2009) c: Chené et al. (2013) d: Shara et al. (2009) e: Hadfield et al. (2007) f: Kurtev et al. (2007) g: Mauerhan et al. (2011) h: van der Hucht (2001) i: Davies et al. (2012b); j: Chené et al. (2015) k: Marston et al. (2013) l: Roman-Lopes (2011) m: Wachter et al. (2010) n: Shara et al. (2012) o: Davies et al. (2012a); p: This work

*: Alternatively WR62-2 and WR62-1 may be associated with WISE H II region G317.236+0.516

with G298 ‘Dragonfish’ complex (Rahman et al. 2011). The VVV CL011 and Mercer 30 clusters are coincident with this region, although radio distances of ~ 10.5 kpc significantly exceed spectrophotometric cluster distances. Similar issues affect the association of Mercer 81 with G338.430+0.048, and VVV CL 041 with G317.030+0.028. Finally, stellar winds and/or supernovae associated with Westerlund 1 have sculpted an IR cavity, such that there is no longer an associated H II region.

Overall, it is apparent that WR stars are rarely located within known H II regions, albeit with some notable exceptions which includes the Carina Nebula in the Milky Way. Typical radii of star-forming regions are 9 arcmin, so for representative radio-derived distances of 7.5 kpc to star forming regions, we include stars within a projected distance of 30 parsec from the centre of the H II region. Again, it is possible that stars have migrated away from where they formed. Typical velocity dispersions of stars in such regions are several km/s, corresponding to several pc/Myr, such that the WR progenitor could have travelled several ten’s of parsec. It is important to stress that the parent star-forming region of a WR star would not necessarily display significant radio

free-free emission after 5–10 Myr (Meynet & Maeder 2003) since most O stars will have died if there had been a single burst of star formation. Indeed, only 23 (46%) of the 50 GOSC optically visible O stars in our survey region lie in an OB association (Cen OB1, Nor OB1, Ara OB1).

Regardless of whether WR progenitors form in clusters or lower density environments, there are other explanations for their relative isolation. To have travelled more than a few 10s of parsec from their birth site, the WR progenitor may have been ejected via dynamical effects or following a supernova kick from a close companion. The former, involving 3-body dynamical interactions, is favoured in dense stellar environments, in which the fraction of massive stars ejected is inversely proportional to the stellar mass of the cluster (Fuji & Portegies Zwart 2011). Therefore, the population of WR stars dynamically ejected in this way will be dominated by those from low to intermediate mass clusters, explaining why the $10^5 M_\odot$ cluster Westerlund 1 has successfully retained the majority of its WR population. Historically, a supernova origin for runaway WR stars has been considered to be a major factor affecting their spatial distribution (Eldridge et al. 2011). This requires a close binary compan-

ion, and assumes that all massive stars whose initial masses exceed $\sim 20M_{\odot}$ undergo a core-collapse SN. Of course, such stars may collapse directly to a black hole, or form a black hole via fallback, so their companion would not necessarily receive a significant supernova kick (e.g. O'Connor & Ott 2011). Therefore, only a small fraction of isolated WR stars likely originate in this way.

Overall, the most promising scenario for the low observed frequency of WR stars associated with star clusters is via dynamical ejection, but this alone doesn't explain the very high fraction of WR stars in the field. Instead, it is likely that a majority of Galactic WR progenitors do not form within dense, high mass star clusters. The observed high fraction of WR stars located in the Galactic field can therefore be attributed to a combination of dynamical ejection from star clusters, and their origins in modest star-forming regions which subsequent dissolve into the field. The latter will not necessarily be recognisable as an OB association during the WR stage since the majority of O stars will have ended their lives after 5–10 Myr, with similar arguments applying to isolated H II regions. Some distant WR stars will not be recognised as being associated with a star forming region if other stars in the region possess low masses, as is the case for γ Vel (Jeffries et al. 2014).

6.2 Relative isolation of WR stars and Luminous Blue Variables

The general lack of association between Wolf-Rayet stars and O stars – except for the minority located in young, dense star clusters (e.g. NGC 3603, Westerlund 1) – is relevant to the ongoing debate about the nature of Luminous Blue Variables (Humphreys et al. 2016; Smith 2016). Historically LBVs were considered to be massive stars in transition towards the WR stage. In part, this association arose from the spectroscopic evolution of LBVs to the WN phase (e.g. AG Car Smith et al. 1994) and LBV outbursts from WN stars (e.g. R127, HDE 269582, Walborn et al. 2017). Smith & Tombleson (2015) have challenged this view, finding that LBVs in the Milky Way and LMC are more isolated (from O stars) than Wolf-Rayet stars. They have argued that they possess lower masses, with their high luminosities arising from being the mass gainers (former secondaries) within close binary systems.

Their conclusions were largely based upon the spatial distribution of O stars, WR stars and LBVs in the LMC, owing to visual studies of Galactic massive stars being severely restricted by dust extinction. Still, the reliance on SIMBAD for catalogues of O stars hinders their conclusions owing to severe incompleteness for both galaxies, while Humphreys et al. (2016) argued for a mass separation between high luminosity (classical) and low luminosity LBVs (though see Smith 2016).

Kniazev et al. (2015, 2016) provide the current census of 17 confirmed LBVs in the Milky Way, which is restricted to confirmed spectroscopic variables. Their criteria therefore exclude candidate LBVs possessing ejecta nebulae, which Bohannan (1997) had previously argued should be an additional discriminator. Only three spectroscopically variable LBVs lie within our Galactic survey region – WS1 (Kniazev et al. 2015), Wray 16-137 (Gvaramadze et al. 2015) and Wd1-W243 (Clark et al. 2005) – so we need to

consider the global Milky Way population of LBVs and WR stars.

Of the known WR content in the Milky Way, 27% are members of star clusters (Crowther 2015). Meanwhile, 4 of the 17 spectroscopically variable LBVs are located in star clusters – W243 in Westerlund 1, η Car in Trumpler 16, GCIRS 34W in the Galactic Centre cluster and qF 362 in the Quintuplet cluster (Geballe et al. 2000) – comprising 24% of the total, so their global statistics are comparable. Indeed, a number of widely accepted LBVs known to be associated with star clusters are omitted from the compilation of Kniazev et al. (2015). These include the Pistol star (qF 134), another member of the Quintuplet cluster (Figer et al. 1998), and the LBV in the 1806-20 cluster (Eikenberry et al. 2004; Figer et al. 2004).

5 of the 17 spectroscopically variable LBVs are potentially associated with star-forming regions (Anderson et al. 2014) from a similar exercise to that discussed above for WR stars, namely η Car, Wray 16-137, HD 168607, AFGL 2298 and G24.73+0.69, namely 29% of the total. Consequently, the overwhelming majority of WR stars and LBVs are located in the Galactic field, away from star clusters or star-forming regions. Overall, there is no significant difference in the spatial distribution of WR and LBVs in our Galaxy, with a quarter of both populations associated with young massive star clusters.

Smith & Tombleson (2015) proposed that LBVs generally arise from significantly lower mass progenitors than WR stars, challenging the hitherto scenario that LBVs are transition objects between the O and WR phases. However, those star clusters which host LBVs are relatively young (4–6 Myr Clark et al. 2005; Bibby et al. 2008; Liermann et al. 2012; Schneider et al. 2014), putting aside η Car⁶. Not only are the statistics of WR and LBV association with star clusters comparable, but crucially 4 young Milky Way clusters hosting LBVs – Westerlund 1, CL 1806-20, the Galactic Centre and the Quintuplet – also contain (classical) WR stars.

Smith & Tombleson (2015) argued that LBVs arise from mass gainers in close binary systems (Langer 2012; de Mink et al. 2014). Mass gainers will be rejuvenated, yielding an apparently younger star than the rest of the population (Schneider et al. 2014). The presence of spectroscopically variable LBVs (Wd1-W243, GCIRS 34W, qF 362) plus leading LBV candidates (qF 134, LBV 1806-20) in young clusters with progenitor masses in the range 30–40 M_{\odot} and coexisting with O stars and WR stars, should permit their scenario to be tested. Of course, LBVs in such systems might be the mass-gaining secondaries whose primaries have already undergone core-collapse. However, LBV 1806-20 is an SB2 system, whose companion is not a WR star since it exhibits He I absorption lines. This appears to rule out the Smith & Tombleson (2015) scenario in this instance.

If LBVs are rejuvenated secondaries in close binaries spanning a wide range of masses, they should also be present in older, massive star clusters such as those hosting large red supergiant (RSG) populations. However,

⁶ η Car is unusual since it is associated with an even younger star cluster, Trumpler 16, which also hosts the massive main-sequence O2.5If/WN6 star WR25 (Massey & Johnson 1993; Crowther & Walborn 2011)

Smith & Tombleson (2015) report that LBVs and RSGs do not share a common parent population, and LBVs are not known within RSG-rich clusters at the base of the Scutum-Crux arm (RSGC 1–3, Figer et al. 2006; Davies et al. 2007; Clark et al. 2009). The presence of ~ 50 RSG in these clusters and absence of LBVs argues either against the Smith & Tombleson (2015) scenario, or requires a short ($\sim 2 \times 10^4$ yr) lifetime for such LBV, in view of the ~ 1 Myr RSG lifetime. The only potential LBV within these RSG rich clusters identified to date is IRAS 18367–0556 in RSGC 2, which possesses a mid-IR ejecta nebula (Davies et al. 2007). Overall, it is apparent that LBVs span a wide range of physical properties (Smith et al. 2004), though the same is true for WR stars, some of which are located in significantly older star clusters (recall Table 9 from C06), albeit solely Westerlund 1 hosts RSG and WR stars.

7 CONCLUSIONS

We have undertaken a near-IR spectroscopic search for Wolf-Rayet stars along the Scutum-Crux spiral arm, based upon 2MASS and GLIMPSE photometric criteria (Mauerhan et al. 2011; Faherty et al. 2014). Observations of 127 candidate stars ($K_S \sim 10 - 13$ mag) resulted in the confirmation of 17 WR stars (14 WN, 3 WC), representing a success rate of $\sim 13\%$, comparable to previous IR-selected studies based on similar criteria (Hadfield et al. 2007; Mauerhan et al. 2011). More sophisticated techniques are clearly required for optimising future spectroscopic searches. As we have found, large numbers of other stellar types (young stellar objects, Be stars) lie in the same location as WR stars within individual colour-colour diagrams, but may not do so in a multi-dimensional parameter space. Therefore, future progress might entail a Bayesian approach to optimising searches for candidate WR stars.

We have extended our earlier near-IR classification scheme (C06) to cover all YJHK bands and all subtypes, including WN/C and WO subtypes. This has been tested on several recently discovered WR stars for which optical classifications have previously been obtained. In general, the near-IR criteria are successful in obtaining reliable subtypes, including the presence of atmospheric hydrogen in WN stars, and identifying transition WN/C stars. However, inferences are weaker if limited wavebands are available, the spectral resolution is modest, and/or the signal-to-noise obtained is low.

The majority of newly discovered WR stars are weak-lined WN5–7 stars, with two broad-lined WN4–6 stars and three WC6–8 stars. Therefore, despite the low success rate, our goal of extending the spectroscopic confirmation of WR stars to the far side of the Milky Way has been successful. Based on the absolute magnitude calibration of C15, inferred distances (~ 10 kpc) extend beyond previous spectroscopic surveys, with $A_{K_S} \sim 1.2$ mag. Spectroscopic searches beyond the Galactic Centre ($A_{K_S} \sim 3$ mag) will be significantly more challenging.

Only a quarter of WR stars in the selected Galactic longitude range are associated with star clusters and/or H II regions. We suggest that this arises from a combination of dynamical ejection from (modest stellar mass) clusters and formation within lower density environments (OB associa-

tions/extended H II regions). We also revisit the recent controversy about the association between LBVs and WR stars, or lack thereof. Considering the whole Milky Way, 27% of WR stars are hosted by clusters, comparable to that of spectroscopically variable LBVs (4 from 17 stars). More significantly, several young clusters with main sequence turn-off masses close to $30\text{--}40 M_\odot$ host classical WR stars and LBVs, permitting Smith & Tombleson (2015)’s suggestion that some LBVs are rejuvenated mass gainers of close binaries to be tested. Specifically, the non-WR companion to LBV 1806-20 and absence of LBVs in RSG-rich star clusters argue against this scenario.

Returning to the main focus of this study, until more robust distances to WR stars - and in turn absolute magnitudes - can be established by *Gaia* there are legitimate concerns about the completeness of surveys for different subtypes, especially the challenge of identifying faint, weak emission line WN stars with respect to WC stars (Massey et al. 2015a). Near-IR narrow-band photometric searches suffer from dilution of emission lines by companion stars and hot dust emission from WC binaries, while our broad-band near to mid-IR photometric approach is limited by the low spatial resolution of Spitzer. Massey et al. (2015b) have undertaken a deep optical narrow-band survey of the LMC, revealing a population of faint, weak-lined WN3 stars (which they characterize as WN3/O3 stars). Stars with these characteristics - which would usually be classified as WN3ha according to the Smith et al. (1996) scheme - comprise a negligible fraction of Galactic WR stars (e.g. WR3), a minority of the moderately metal-poor LMC WR population, and a majority of the more significantly metal deficient SMC WR population (Hainich et al. 2015).

It is anticipated that ongoing infrared searches using a combination of continuum methods and emission line characteristics will significantly improve the completeness of WR surveys in a sizeable volume of the Galaxy within the near future.

ACKNOWLEDGMENTS

We wish to thank Nicole Homeier, Bill Vacca and Frank Tramper for providing us with near-IR spectroscopic datasets, from NTT/SOFI, IRTF/SpeX and VLT/XSHOOTER respectively, for several WR stars. We appreciate useful discussions with Simon Goodwin and Richard Parker, and useful comments from the referee which helped improve the focus of the paper. Financial support for CKR was provided by the UK Science and Technology Facilities Council. PAC would like to thank ESO for arranging emergency dental care in La Serena immediately after the 2015 observing run.

REFERENCES

- Acker A., Stenholm B., 1990, *A&AS*, **86**, 219
- Anderson L. D., Bania T. M., Balser D. S., Cunningham V., Wenger T. V., Johnstone B. M., Armentrout W. P., 2014, *ApJS*, **212**, 1
- Benjamin R. A., et al., 2003, *PASP*, **115**, 953
- Bibby J. L., Crowther P. A., Furness J. P., Clark J. S., 2008, *MNRAS*, **386**, L23

- Bohannon B., 1997, in Nota A., Lamers H., eds, ASP Conf Ser Vol. 120, Luminous Blue Variables: Massive Stars in Transition. p. 3
- Bohannon B., Crowther P. A., 1999, *ApJ*, **511**, 374
- Borissova J., et al., 2011, *A&A*, **532**, A131
- Bressert E., et al., 2010, *MNRAS*, **409**, L54
- Chené A.-N., et al., 2013, *A&A*, **549**, A98
- Chené A.-N., et al., 2015, *A&A*, **584**, A31
- Churchwell E., et al., 2006, *ApJ*, **649**, 759
- Clark J. S., Negueruela I., Crowther P. A., Goodwin S. P., 2005, *A&A*, **434**, 949
- Clark J. S., et al., 2009, *A&A*, **498**, 109
- Cooper H. D. B., et al., 2013, *MNRAS*, **430**, 1125
- Crowther P. A., 2000, *A&A*, **356**, 191
- Crowther P. A., 2007, *ARA&A*, **45**, 177
- Crowther P. A., 2015, in Hamann W.-R., Sander A., Todt H., eds, Wolf-Rayet Stars: Proceedings of an International Workshop, Universitätsverlag Potsdam, p.21-26. pp 21–26 ([arXiv:1509.00495](https://arxiv.org/abs/1509.00495))
- Crowther P. A., Smith L. J., 1996, *A&A*, **305**, 541
- Crowther P. A., Walborn N. R., 2011, *MNRAS*, **416**, 1311
- Crowther P. A., Smith L. J., Willis A. J., 1995, *A&A*, **304**, 269
- Crowther P. A., Hadfield L. J., Clark J. S., Negueruela I., Vacca W. D., 2006, *MNRAS*, **372**, 1407
- Dalton G., et al., 2016, in Ground-based and Airborne Instrumentation for Astronomy VI. p. 99081G, [doi:10.1117/12.2231078](https://doi.org/10.1117/12.2231078)
- Davies B., Figer D. F., Kudritzki R.-P., MacKenty J., Najarro F., Herrero A., 2007, *ApJ*, **671**, 781
- Davies B., de La Fuente D., Najarro F., Hinton J. A., Trombley C., Figer D. F., Puga E., 2012a, *MNRAS*, **419**, 1860
- Davies B., et al., 2012b, *MNRAS*, **419**, 1871
- Dias W. S., Alessi B. S., Moitinho A., Lépine J. R. D., 2002, *A&A*, **389**, 871
- Dutra C. M., Bica E., Soares J., Barbuy B., 2003, *A&A*, **400**, 533
- Eenens P. R. J., Williams P. M., 1994, *MNRAS*, **269**, 1082
- Eenens P. R. J., Williams P. M., Wade R., 1991, *MNRAS*, **252**, 300
- Eikenberry S. S., et al., 2004, *ApJ*, **616**, 506
- Eldridge J. J., Langer N., Tout C. A., 2011, *MNRAS*, **414**, 3501
- Faherty J. K., Shara M. M., Zurek D., Kanarek G., Moffat A. F. J., 2014, *AJ*, **147**, 115
- Figer D. F., McLean I. S., Najarro F., 1997, *ApJ*, **486**, 420
- Figer D. F., Najarro F., Morris M., McLean I. S., Geballe T. R., Ghez A. M., Langer N., 1998, *ApJ*, **506**, 384
- Figer D. F., Najarro F., Kudritzki R. P., 2004, *ApJ*, **610**, L109
- Figer D. F., MacKenty J. W., Robberto M., Smith K., Najarro F., Kudritzki R. P., Herrero A., 2006, *ApJ*, **643**, 1166
- Fujii M. S., Portegies Zwart S., 2011, *Science*, **334**, 1380
- Gaia Collaboration et al., 2016, *A&A*, **595**, A2
- Geballe T. R., Najarro F., Figer D. F., 2000, *ApJ*, **530**, L97
- Georgelin Y. M., Georgelin Y. P., 1976, *A&A*, **49**, 57
- Gvaramadze V. V., Kniazev A. Y., Berdnikov L. N., 2015, *MNRAS*, **454**, 3710
- Hadfield L. J., van Dyk S. D., Morris P. W., Smith J. D., Marston A. P., Peterson D. E., 2007, *MNRAS*, **376**, 248
- Hainich R., Pasemann D., Todt H., Shenar T., Sander A., Hamann W.-R., 2015, *A&A*, **581**, A21
- Hénault-Brunet V., et al., 2012, *A&A*, **546**, A73
- Hillier D. J., Jones T. J., Hyland A. R., 1983, *ApJ*, **271**, 221
- Homeier N. L., Blum R. D., Pasquali A., Conti P. S., Daminieli A., 2003, *A&A*, **408**, 153
- Hopewell E. C., et al., 2005, *MNRAS*, **363**, 857
- Howarth I. D., Schmutz W., 1992, *A&A*, **261**, 503
- Humphreys R. M., Weis K., Davidson K., Gordon M. S., 2016, *ApJ*, **825**, 64
- Jeffries R. D., et al., 2014, *A&A*, **563**, A94
- Kanarek G., Shara M., Faherty J., Zurek D., Moffat A., 2015, *MNRAS*, **452**, 2858
- Kniazev A. Y., Gvaramadze V. V., Berdnikov L. N., 2015, *MNRAS*, **449**, L60
- Kniazev A. Y., Gvaramadze V. V., Berdnikov L. N., 2016, *MNRAS*, **459**, 3068
- Kothes R., Dougherty S. M., 2007, *A&A*, **468**, 993
- Koumpia E., Bonanos A. Z., 2012, *A&A*, **547**, A30
- Kurtev R., Borissova J., Georgiev L., Ortolani S., Ivanov V. D., 2007, *A&A*, **475**, 209
- Langer N., 2012, *ARA&A*, **50**, 107
- Larson R. B., 2003, in De Buizer J. M., van der Blik N. S., eds, ASP Conf Ser Vol. 287, Galactic Star Formation Across the Stellar Mass Spectrum. pp 65–80 ([arXiv:astro-ph/0205466](https://arxiv.org/abs/astro-ph/0205466))
- Liermann A., Hamann W.-R., Oskinova L. M., 2009, *A&A*, **494**, 1137
- Liermann A., Hamann W.-R., Oskinova L. M., 2012, *A&A*, **540**, A14
- Lundstrom I., Stenholm B., 1984, *A&AS*, **58**, 163
- Maíz Apellániz J., et al., 2013, in Massive Stars: From alpha to Omega. p. 198 ([arXiv:1306.6417](https://arxiv.org/abs/1306.6417))
- Marston A., Mauerhan J. C., Van Dyk S., Cohen M., Morris P., 2013, in Massive Stars: From alpha to Omega. p. 167 ([arXiv:1309.1584](https://arxiv.org/abs/1309.1584))
- Massey P., Johnson J., 1993, *AJ*, **105**, 980
- Massey P., Neugent K. F., Morrell N., Hillier D. J., 2014, *ApJ*, **788**, 83
- Massey P., Neugent K. F., Morrell N. I., 2015a, in Hamann W.-R., Sander A., Todt H., eds, Wolf-Rayet Stars: Proceedings of an International Workshop, Universitätsverlag Potsdam, p.35-42. pp 35–42 ([arXiv:1507.07297](https://arxiv.org/abs/1507.07297))
- Massey P., Neugent K. F., Morrell N., 2015b, *ApJ*, **807**, 81
- Mauerhan J. C., Van Dyk S. D., Morris P. W., 2009, *PASP*, **121**, 591
- Mauerhan J. C., Muno M. P., Morris M. R., Stolovy S. R., Cotera A., 2010, *ApJ*, **710**, 706
- Mauerhan J. C., Van Dyk S. D., Morris P. W., 2011, *AJ*, **142**, 40
- Mercer E. P., et al., 2005, *ApJ*, **635**, 560
- Messineo M., Menten K. M., Churchwell E., Habing H., 2012, *A&A*, **537**, A10
- Meynet G., Maeder A., 2003, *A&A*, **404**, 975
- Miszalski B., Mikołajewska J., Udalski A., 2013, *MNRAS*, **432**, 3186
- Najarro F., de la Fuente D., Geballe T. R., Figer D. F., Hillier D. J., 2015, in Hamann W.-R., Sander A., Todt H., eds, Wolf-Rayet Stars: Proceedings of an International Workshop, Universitätsverlag Potsdam, p.113-116. pp 113–116
- Nebot Gómez-Morán A., Motch C., Pineau F.-X., Carrera F. J., Pakull M. W., Riddick F., 2015, *MNRAS*, **452**, 884
- O’Connor E., Ott C. D., 2011, *ApJ*, **730**, 70
- Parker R. J., Dale J. E., 2017, preprint, ([arXiv:1705.04686](https://arxiv.org/abs/1705.04686))
- Parker R. J., Goodwin S. P., 2007, *MNRAS*, **380**, 1271
- Porter J. M., Drew J. E., Lumsden S. L., 1998, *A&A*, **332**, 999
- Rahman M., Moon D.-S., Matzner C. D., 2011, *ApJ*, **743**, L28
- Roman-Lopes A., 2011, *MNRAS*, **410**, 161
- Rosslowe C. K., Crowther P. A., 2015a, *MNRAS*, **447**, 2322
- Rosslowe C. K., Crowther P. A., 2015b, *MNRAS*, **449**, 2436
- Rousselot P., Lidman C., Cuby J.-G., Moreels G., Monnet G., 2000, *A&A*, **354**, 1134
- Russeil D., 2003, *A&A*, **397**, 133
- Russeil D., Adami C., Amram P., Le Coarer E., Georgelin Y. M., Marcellin M., Parker Q., 2005, *A&A*, **429**, 497
- Sagar R., Munari U., de Boer K. S., 2001, *MNRAS*, **327**, 23
- Sana H., et al., 2012, *Science*, **337**, 444
- Sander A., Hamann W.-R., Todt H., 2012, *A&A*, **540**, A144
- Schneider F. R. N., et al., 2014, *ApJ*, **780**, 117
- Shara M. M., Moffat A. F. J., Smith L. F., Niemela V. S., Potter M., Lamontagne R., 1999, *AJ*, **118**, 390
- Shara M. M., et al., 2009, *AJ*, **138**, 402

- Shara M. M., Faherty J. K., Zurek D., Moffat A. F. J., Gerke J., Doyon R., Artigau E., Drissen L., 2012, *AJ*, 143, 149
- Simpson R. J., et al., 2012, *MNRAS*, 424, 2442
- Skrutskie M. F., Cutri R. M., Stiening R., Weinberg M. D., Schneider S., Carpenter J. M., Beichman C., Capps R. e. a., 2006, *AJ*, 131, 1163
- Smith N., 2016, *MNRAS*, 461, 3353
- Smith N., Tombleson R., 2015, *MNRAS*, 447, 598
- Smith L. F., Shara M. M., Moffat A. F. J., 1990, *ApJ*, 358, 229
- Smith L. J., Crowther P. A., Prinja R. K., 1994, *A&A*, 281, 833
- Smith L. F., Shara M. M., Moffat A. F. J., 1996, *MNRAS*, 281, 163
- Smith N., Vink J. S., de Koter A., 2004, *ApJ*, 615, 475
- Stead J. J., Hoare M. G., 2009, *MNRAS*, 400, 731
- Toalá J. A., Guerrero M. A., Ramos-Larios G., Guzmán V., 2015, *A&A*, 578, A66
- Tramper F., et al., 2015, *A&A*, 581, A110
- Vallée J. P., 2014, *ApJS*, 215, 1
- Vallée J. P., 2015, *MNRAS*, 450, 4277
- Vreux J. M., Dennefeld M., Andrillat Y., 1983, *A&AS*, 54, 437
- Vreux J.-M., Andrillat Y., Biemont E., 1990, *A&A*, 238, 207
- Wachter S., Mauerhan J. C., Van Dyk S. D., Hoard D. W., Kafka S., Morris P. W., 2010, *AJ*, 139, 2330
- Walborn N. R., Gamen R. C., Morrell N. I., Barbá R. H., Fernández Lajús E., Angeloni R., 2017, *AJ*, 154, 15
- Weidner C., Kroupa P., Bonnell I. A. D., 2010, *MNRAS*, 401, 275
- Wright N. J., Bouy H., Drew J. E., Sarro L. M., Bertin E., Cuillandre J.-C., Barrado D., 2016, *MNRAS*, 460, 2593
- de Jong R. S., et al., 2016, in *Ground-based and Airborne Instrumentation for Astronomy VI*. p. 99081O, doi:10.1117/12.2232832
- de Mink S. E., Sana H., Langer N., Izzard R. G., Schneider F. R. N., 2014, *ApJ*, 782, 7
- de la Fuente D., Najarro F., Trombly C., Davies B., Figer D. F., 2015, *A&A*, 575, A10
- van der Hucht K. A., 2001, *New Astron. Rev.*, 45, 135

SUPPLEMENTARY INFORMATION

Additional information may be found in the online version of this article:

Appendix A: Near-IR spectral classification of WR stars

Appendix B: Spectroscopic observations of IR selected candidates

Please note: Oxford University Press is not responsible for the content or functionality of any supporting materials supplied by the authors. Any queries (other than missing material) should be directed to the corresponding author for this article.

APPENDIX A: NEAR-IR SPECTRAL CLASSIFICATION OF WR STARS

C06 utilised $\text{He II } 1.012\mu\text{m}/\text{He I } 1.083\mu\text{m}$ and $\text{C IV } 1.19\mu\text{m}/\text{C III } 1.20\mu\text{m}$ to classify WN and WC stars from YJ-band spectroscopy, respectively, plus $\text{He II } 2.189\mu\text{m}/\text{Br}\gamma$ and $\text{C IV } 2.08\mu\text{m}/\text{C III } 2.11\mu\text{m}$ from K-band spectroscopy. Subtypes for weak/narrow WN4–7 stars with a $\text{He II } 1.01\mu\text{m}$ FWHM $\leq 65\text{\AA}$ were distinguished by the ratio of $\text{N V } 2.10\mu\text{m}/(\text{He I} + \text{N III } 2.11\mu\text{m})$, while WC8–9 stars were also classified from their $\text{C III } 0.97\mu\text{m}/\text{C II } 0.99\mu\text{m}$ ratio. However, separating broad-lined WN4–7 stars and WC5–7 stars from near-IR spectroscopy proved to be extremely challenging. In addition, the use of $\text{He II } 2.189\mu\text{m}/\text{Br}\gamma$ as a classification diagnostic adds a further complication owing to the sensitivity of this ratio on hydrogen content as well as ionization. Consequently, we revisit these issues in the following discussion.

A1 WN stars

The primary classification diagnostics of WN stars involve helium ($\text{He II } 5411/\text{He I } 5876$) and nitrogen ($\text{N III } 4640$, $\text{N IV } 4058$, $\text{N V } 4610$) lines, with strong, broad-lined WN stars (WNb or WN-s) further distinguished from weak narrow-lined stars (WN, WN-w). In common with C06, we identify strong/broad WN stars with $W_\lambda(\text{He II } 5411) \geq 40\text{\AA}$, and $\text{FWHM}(\text{He II } 4686) \geq 30\text{\AA}$ (Smith et al. 1996) using the FWHM of prominent He II lines, $1.012\mu\text{m}$ and/or $2.189\mu\text{m}$, namely $\geq 1900 \text{ km s}^{-1}$ for WNb stars, plus an equivalent width threshold of $W_\lambda \sim 250\text{\AA}$ for $\text{He II } 1.0124\mu\text{m}$, and/or $W_\lambda \sim 75\text{\AA}$ for $\text{He II } 2.1885\mu\text{m}$.

Central to the optical classification scheme are the ratios of $\text{N III } 4636\text{--}41$, $\text{N IV } 4068$ and $\text{N V } 4603\text{--}20$ lines. At near-IR wavelengths, nitrogen lines are scarce, weak, and often blended with helium lines. The most prominent nitrogen features arise from $\text{N V } (1.111, 1.552, 2.100\mu\text{m})$ in early WN subtypes, although these recombination lines require high S/N spectroscopy for broad-lined stars. In addition, $\text{N III } 2.116$ is prominent in late WN stars, albeit severely blended with $\text{He I } 2.112\text{--}2.113\mu\text{m}$ and/or $\text{C III } 2.115\mu\text{m}$ for WN/C stars.

Consequently we are largely reliant upon the relative strengths of helium lines for IR classification. In the YJ-band, $\text{He II } 1.012\mu\text{m}/\text{He I } 1.083\mu\text{m}$ represents an excellent classification diagnostic for most WN subtypes. $\text{He I } 1.0830$ is blended with $\text{P}\gamma$ (+ $\text{He II } 1.093\mu\text{m}$) in early subtypes and broad-lined stars, while $\text{He II } 1.0124$ is blended with $\text{P}\delta$ (+ $\text{He II } 1.0045\mu\text{m}$) in broad-lined WN stars. Divisions between subtypes are assigned using optically classified WN stars, although broad-lined WN stars cannot be distinguished from this diagnostic.

$\text{He II } 1.692\mu\text{m}/\text{He I } 1.700\mu\text{m}$ provides a H-band diagnostic in narrow-lined WN stars, especially for late subtypes, although blending severely hinders its role in broad-lined stars. Figure A3 compares these ratios in WN stars, indicating that they are well correlated for most narrow-lined WN subtypes.

In the K-band, the relative strengths of $\text{N III } 2.116\mu\text{m}$ (+ $\text{He I } 2.112\text{--}2.113$) to $\text{N V } 2.100\mu\text{m}$ (or $\text{He II } 2.189$) provide key diagnostics in weak-lined WN stars, although this is hindered at low spectral resolution and signal-to-noise since

these emission lines are generally weak. Other relevant pairs of diagnostics, $\text{He II } 1.162/\text{P}\beta$ and $\text{He II } 2.189/\text{Br}\gamma$ provide a combination of ionization and hydrogen content information, so if classifications can be established from other diagnostics, these are helpful in distinguishing hydrogen-rich from hydrogen-deficient WN stars.

A1.1 Hydrogen content

Conti et al. (1983) and Smith et al. (1996) employed the Pickering-Balmer series to characterize the hydrogen content of WN stars, the latter introducing ‘o’, ‘h’ and ‘h’ subtypes for narrow-lined WN stars based on the strength of $\text{H}\beta$ + $\text{He II } 4859$ (8-4) with respect to adjacent Pickering series members $\text{He II } \lambda 5411$ (7-4) and $\text{He II } \lambda 4541$ (9-4), with ‘o’ omitted for broad-lined WN stars. To date, no attempts have been made to develop similar criteria from near-IR series (e.g. Paschen, Brackett), largely because there are additional complications with respect to optical diagnostics.

Firstly, leading He II near-IR lines are blended with other He II series (incl. $n=7$) whose contributions need to be taken into account (e.g. $1.488\mu\text{m}$ 14-7 with $1.476\mu\text{m}$ 9-6). Secondly, hydrogenic He I emission contributes significantly to the hydrogen lines (e.g. $\text{He I } 5\text{--}3$ at $\text{P}\beta$). The former issue can be overcome fairly easily, since medium resolution spectroscopy of late WN stars WR120 and WR123 (dataset U6 from Table 2) reveals $W_\lambda(\text{He II } 1.167)/W_\lambda(1.163) \sim 0.35$ and $W_\lambda(\text{He II } 1.488)/W_\lambda(1.476) \sim 0.35$. However, contributions from neutral helium lines to hydrogen features are more problematic. By way of example, one would expect the observed equivalent width of $1.28\mu\text{m}$ to be $\sim 10\text{\AA}$ for the hydrogen-free WN8 star WR123 (Crowther et al. 1995b) if $\text{He II } (10\text{--}6)$ is the dominant contributor, since $W_\lambda(\text{He II } 11\text{--}6) = 9.4 \pm 0.2\text{\AA}$ and $W_\lambda(\text{He II } 9\text{--}6) = 11.5 \pm 0.6\text{\AA}$, whereas $W_\lambda(1.281\mu\text{m } \text{He II} + \text{P}\beta + \text{He I } 5\text{--}3) = 70 \pm 1\text{\AA}$. Similar issues affect $\text{P}\gamma$ and its adjacent He II lines, $1.042\mu\text{m}$ (13-6) and $1.167\mu\text{m}$ (11-6). Therefore, it is not straightforward to determine the hydrogen content in low ionization WN stars from the Paschen series and their adjacent He II lines.

Instead, we compare the equivalent width ratios of $\text{He I } 1.08\mu\text{m}/\text{He II } 1.01\mu\text{m}$ (ionization) to $\text{P}\beta/\text{He II } 1.16\mu\text{m}$ (ionization and hydrogen content) for narrow-lined WN stars in Fig. A4(a), and broad-lined WN stars in Fig. A4(b). WN stars with optical (h) or ‘h’ classifications are indicated by cross (narrow-lined) or plus (broad-lined) symbols. It is apparent that WN stars with hydrogen exhibit excess $\text{P}\beta$ strengths at a given ionization, such that we have overlaid a pale shaded region for those stars with hydrogen classifications. A darker shaded region, vertically offset by 0.3 dex corresponds to stars with significant hydrogen. Stars close to the boundary include WR66 (WN8(h)) for which Hamann et al. (2006) have obtained 5% atmospheric hydrogen. We have adopted the same criteria for broad-lined WN stars, for which WR136, the only Galactic WNb star with some atmospheric hydrogen in our sample (Crowther & Smith 1996) sits close to the threshold, as does BAT2 (WN2b(h)), for which Hainich et al. (2014) obtained a negligible hydrogen content.

At longer wavelengths, the Brackett series and adjacent He II lines are not easily amenable to the determination of hydrogen content. However, we also consider the equivalent width ratios of $\text{He I } 1.08\mu\text{m}/\text{He II } 1.01\mu\text{m}$ (ionization)

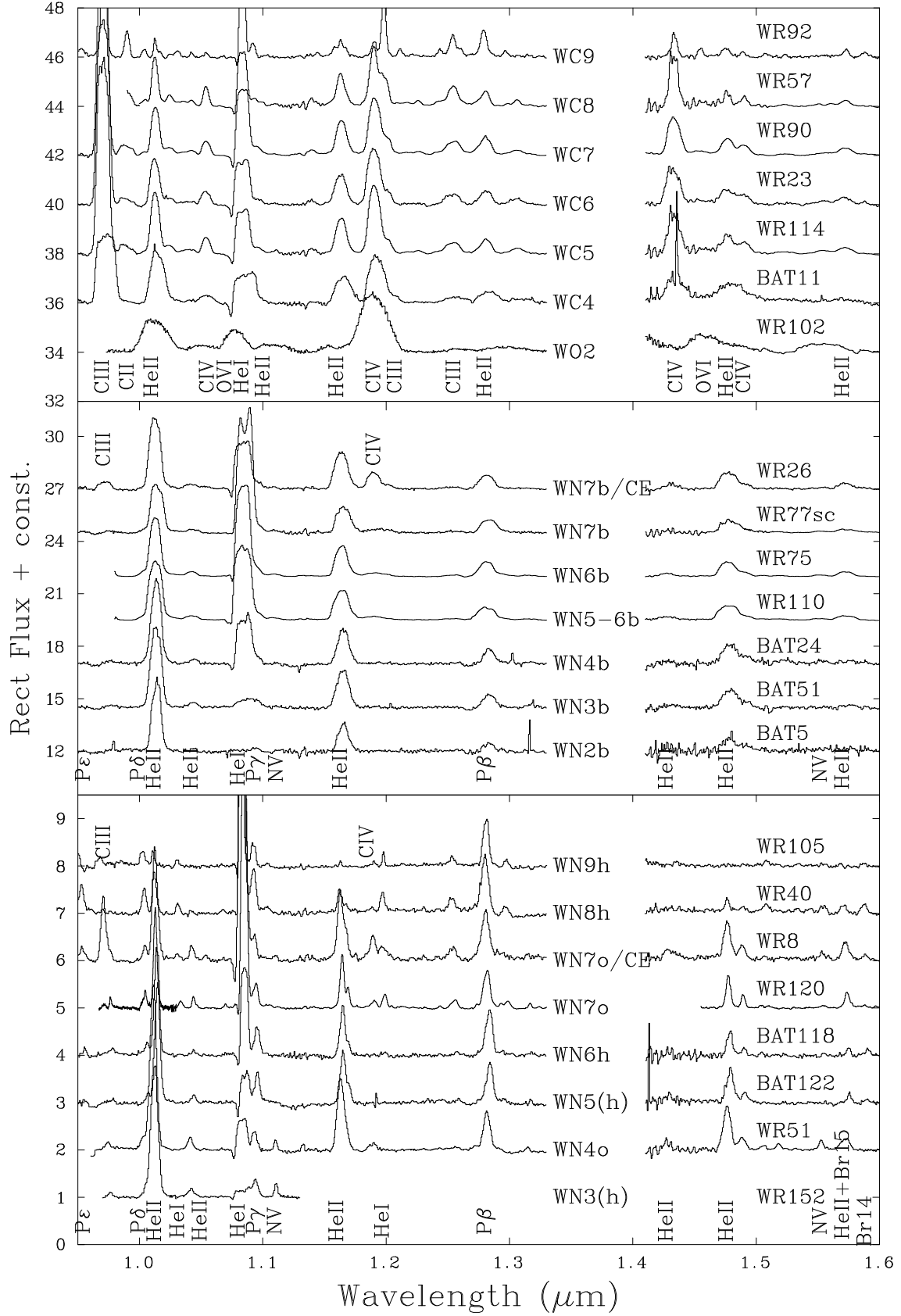


Figure A1. YJ-band spectroscopy of template Galactic and LMC Wolf-Rayet stars, from the present NTT/SOFI dataset, supplemented by archival spectroscopy from various telescopes/instruments. CIV $1.19\mu\text{m}$ and CIII $0.97\mu\text{m}$ are visible in the transition WN7/CE stars WR8 and WR26.

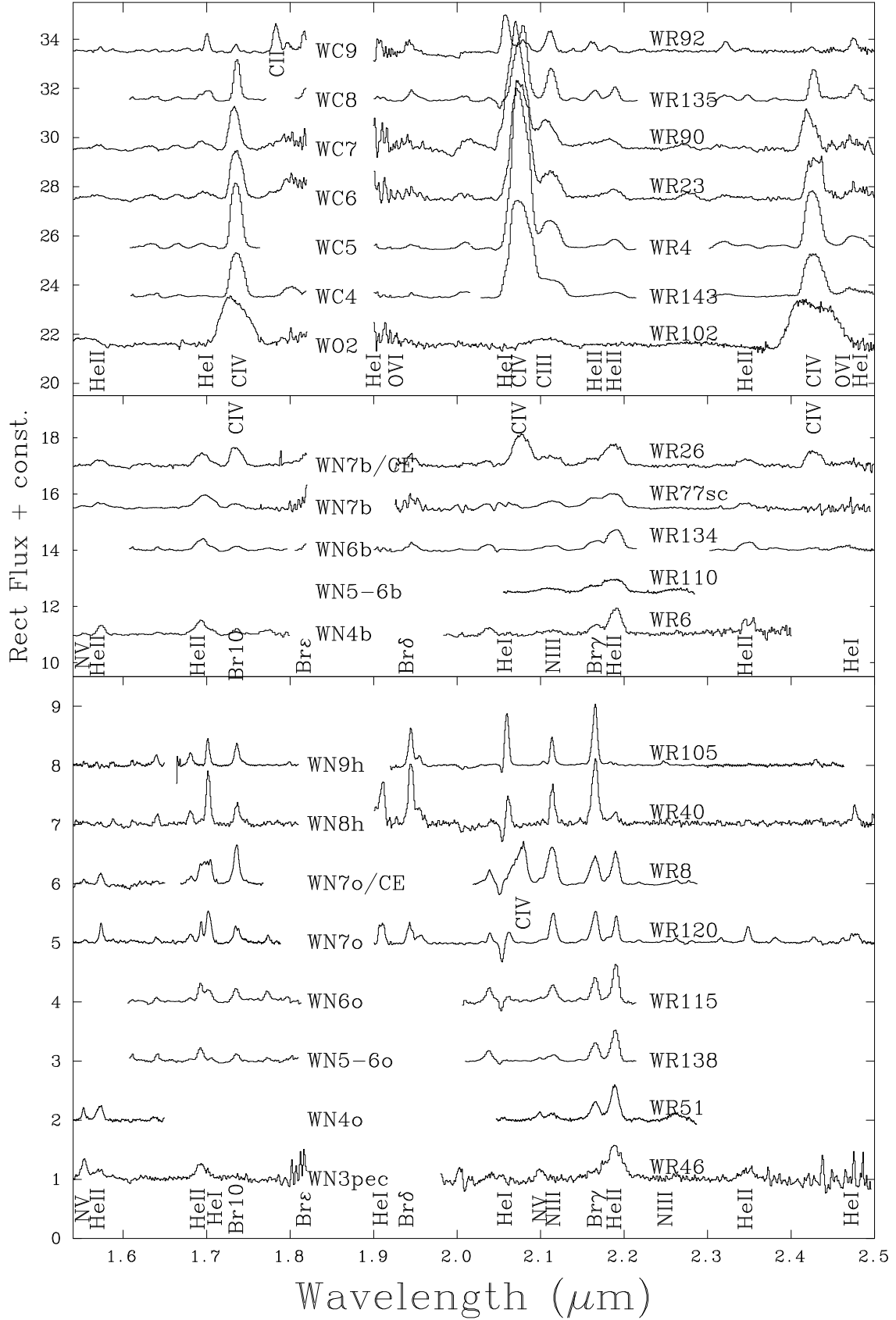


Figure A2. HK-band spectroscopy of template Galactic and LMC Wolf-Rayet stars, from the present NTT/SOFI dataset, supplemented by archival spectroscopy from various telescopes/instruments. C IV 1.74 μ m, 2.07 μ m and 2.43 μ m are prominent in the transition WN7/CE stars WR8 and WR26.

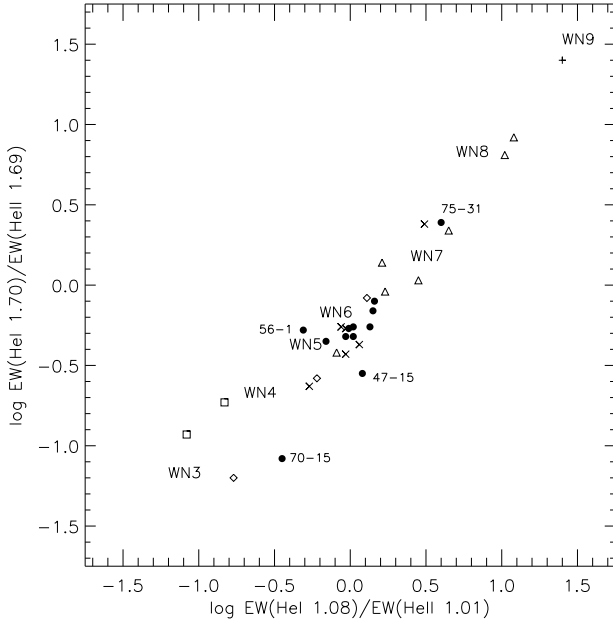


Figure A3. Comparison between He I 1.08 μ m/He II 1.01 μ m and He I 1.70 μ m/He II 1.69 μ m ratios for WN9 (plus symbol), WN7–8 (triangles), WN5–6 stars (diamonds) and WN3–4 stars (squares), with newly identified WN stars indicated as filled circles, and strong-lined WN stars shown as crosses (He I 1.70 and He II 1.69 are severely blended).

to Br γ /He II 2.19 μ m (ionization and hydrogen content) for narrow-lined WN stars in Fig. A4(c), and broad-lined WN stars in Fig. A4(d). These closely resemble the above comparisons, and we have attempted to indicate the regions of stars with atmospheric hydrogen, although high ionization, weak-lined WN3–4 stars with modest hydrogen content (e.g. WR128, WR152 Crowther et al. 1995c) are less straightforward to interpret since they lie close to the boundary. Amongst broad-lined WN stars, WR136 again lies close to the threshold obtained from narrow-line stars.

We have also utilised the He I 1.70 μ m/He II 1.69 μ m ratio together with Br γ /2.189 μ m He II. In Fig. A4(e) and (f) we present a comparison between these equivalent width ratios for narrow-lined and broad-lined WN stars, respectively. Fewer stars are available for this comparison owing to the lack of HK-band spectroscopy for LMC WN stars and the difficulty in deblending He I 1.70 μ m/He II 1.69 μ m, especially in broad-lined stars. Nevertheless, WN(h) and WNh stars again exhibit an excess in Br γ at a given ionization, once again with the notable exception of weak-lined WN3–4(h) stars. The shaded region in Fig. A4(e) indicates regions for which hydrogen is present, which are duplicated for broad-lined stars in Fig. A4(f), with WR136 (WN6b(h)) again close to this threshold.

For WN stars with exceptionally high interstellar reddening, establishing hydrogen contents of WN stars solely from K-band spectroscopy is extremely challenging. This is illustrated in Fig. A5, in which we compare the equivalent width ratios of (N V 2.10 + He I + N III 2.11)/He II 2.19 to Br γ /He II 2.19 μ m. These are ratios are well correlated, although a Br γ excess is generally apparent in WN(h) and WNh stars (crosses and plus symbols), such that we have

indicated these in the shaded region, although no attempt has been made to distinguish between modest and high hydrogen contents from these ratios.

A2 WN/C stars

At visual wavelengths, intermediate WN/C stars usually closely resemble WN stars, albeit with prominent C IV 5808Å emission and usually weakly enhanced carbon recombination lines with respect to helium recombination lines (e.g. C IV 5471/He II 5411). The most prominent carbon lines at near-IR wavelengths are C IV 1.19, 1.74, 2.075, 2.43 μ m, plus C III 0.971, 2.115 μ m. We have identified several pairs of carbon to helium lines amenable to the identification of WN/C stars at near-IR wavelengths, from spectroscopy of transition stars WR8, WR26, WR98, WR145 and BAT88.

In Fig. A6(a) we compare the ratios of C III 0.97 μ m/He II 1.01 μ m to C IV 1.19 μ m/He II 1.16 μ m for WN (squares), WN/C (diamonds) and WC (triangles) stars. The intermediate carbon-to-helium abundances of WN/C stars are reflected in their high C IV 1.19 μ m/He II 1.16 μ m ratios, although only late WN/C subtypes also exhibit elevated C III 0.97 μ m/He II 1.01 μ m ratios, since C III 0.97 μ m is not observed in early-type WN/C stars (e.g. BAT88, WN4b/CE). Nevertheless, C IV 1.19/He II 1.16 is significantly larger in BAT88 with respect to normal WN4b stars (e.g. WR6, WR18).

The only suitable pair of carbon-to-helium recombination lines in the K-band is C IV 2.43 μ m/He II 2.35 μ m, although C IV 2.07 μ m is often also pronounced in WN/C stars (recall WR8 and WR26 in Fig. A2). We therefore consider the ratio of C IV 2.07 μ m/(C III + N III + He I 2.11 μ m), although C III 2.115 μ m will also be enhanced at late subtypes. Fig. A6(b) compares these ratios in WN/C stars with WN and WC stars. WN/C stars are well separated from most normal subtypes with the notable exceptions of WC9 stars which have unusually weak C IV emission lines (and strong C III 2.11 μ m emission), but are otherwise easily distinguished from transition WN/C stars.

Finally, C IV 1.74 μ m/(He II 1.69 + He I 1.70) is also a potential diagnostic, although this is complicated by the presence of Br10 + He II 1.735 in late WN stars such that it is most effective in hydrogen-free early subtypes. By way of example, C IV 1.74 μ m is enhanced in WR8 (WN7o/CE) with respect to WR120 (WN7o) in Fig. A2.

A3 WC stars

For WC stars, the primary optical diagnostics involve the ratio of C IV 5808Å/C III 5696Å, with other secondary criteria - O III-v 5592Å for early WC stars according to Smith et al. (1990) and C II 4267Å for late WC stars according to Crowther et al. (1998). In sharp contrast with WN stars, there are many carbon lines observed in the near-IR spectra of WC stars (Eenens et al. 1991), the strongest of which include C II 0.990, 1.785 μ m, C III 0.971, 1.199, 2.115 μ m, C IV 1.190, 1.430, 1.736, 2.075 and 2.427 μ m. Prominent helium lines include He I 1.08, 1.70, and He II 1.01, 1.16 μ m, although C IV contributes significantly to lines which otherwise would be assumed to correspond to solely ionized helium, i.e. C IV (10–8) to He II (5–4) at 1.01 μ m.

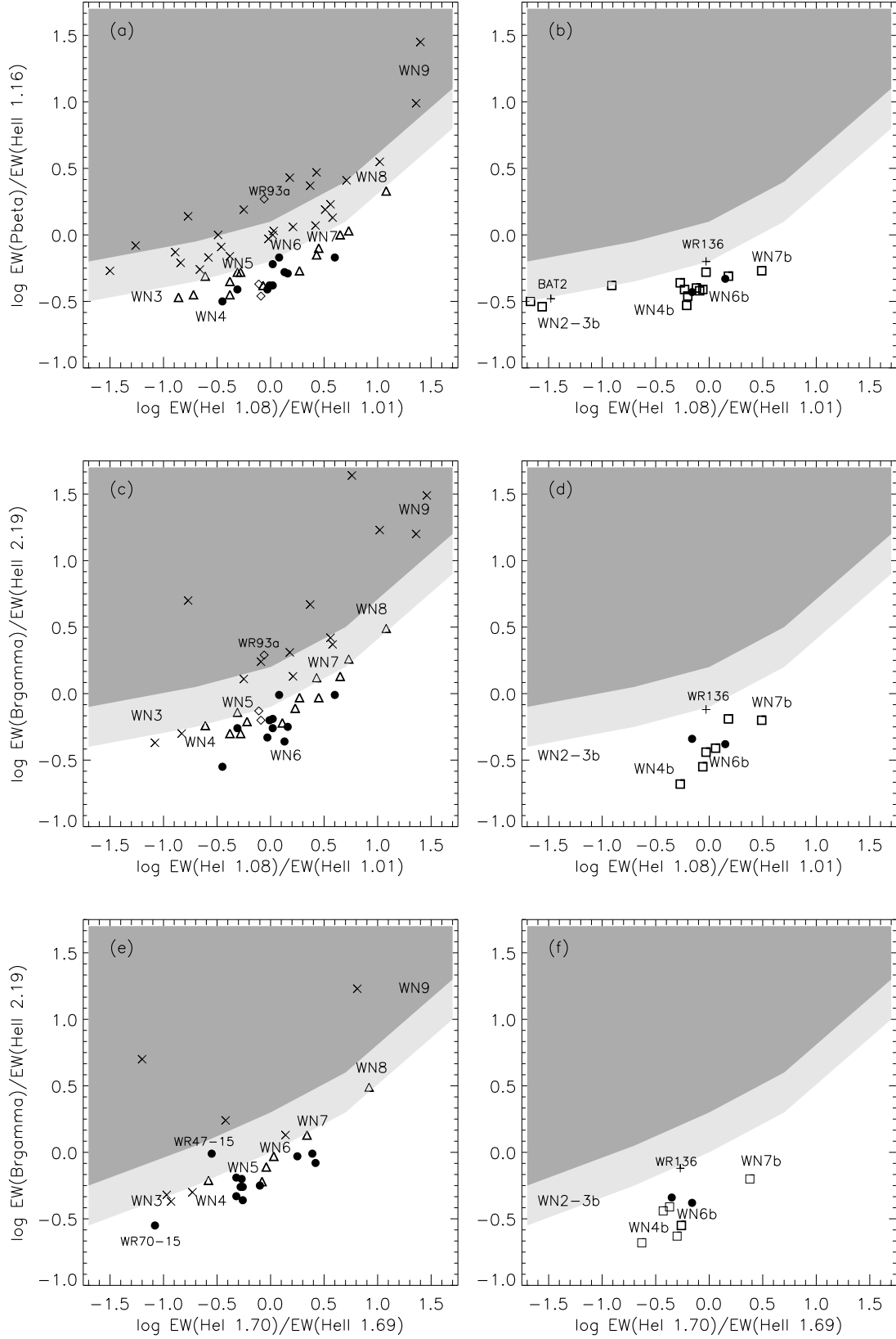


Figure A4. (a): Comparison between He I $1.08\mu\text{m}$ /He II $1.01\mu\text{m}$ and P β /He II $1.16\mu\text{m}$ ratios for narrow-lined WN stars (hydrogen-free: triangles; hydrogen: crosses), with the pale (dark) shaded regions indicating modest (high) hydrogen contents. Newly discovered WN stars are indicated by filled circles while previously discovered WN stars lacking previous optical classifications (WR62a, 68a, 93a) are indicated by diamonds; (b) as (a) for broad-lined WN stars (hydrogen-free: squares; hydrogen: pluses). (c) Comparison between He I $1.08\mu\text{m}$ /He II $1.01\mu\text{m}$ and Br γ /He II $2.19\mu\text{m}$ ratios for narrow-lined WN stars, symbols as for (a); (d) as (c) for broad-lined WN stars, symbols as in (b). (e) Comparison between He I $1.70\mu\text{m}$ /He II $1.69\mu\text{m}$ and Br γ /He II $2.19\mu\text{m}$ ratios for narrow-lined WN stars, symbols as for (a); (f) as (e) for broad-lined WN stars, symbols as for (b).
MNRAS **000**, 1–30 (2017)

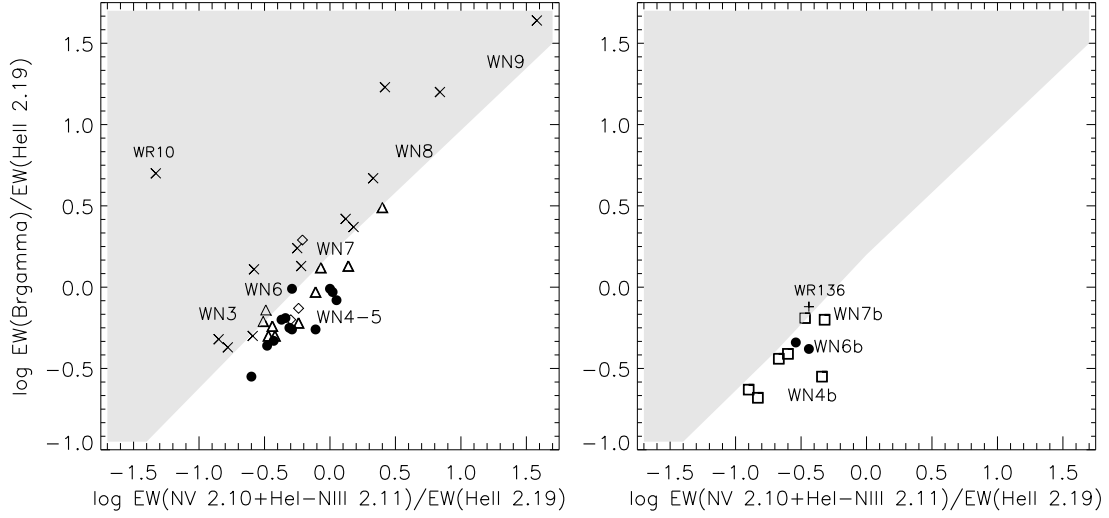


Figure A5. **Left panel** Comparison between $(\text{N v } 2.10\mu\text{m} + \text{He I} + \text{N III } 2.11\mu\text{m})/\text{He II } 2.19\mu\text{m}$ and $\text{Br}\gamma/\text{He II } 2.19\mu\text{m}$ ratios for narrow-lined WN stars, symbols as in Fig. A4(a). The shaded region indicates the approximate domain of WN stars with hydrogen. WR10 is a WN5ha star with extremely weak 2.10-2.11 μm emission. **Right panel** Comparison for broad-lined WN stars, symbols as in Fig. A4(b).

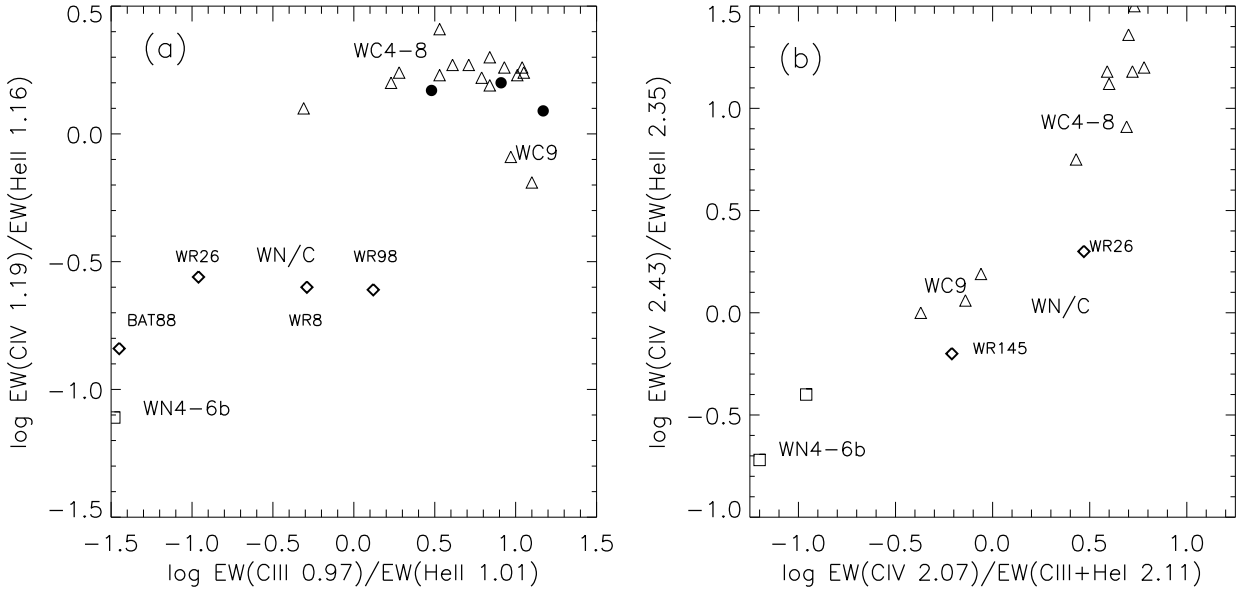


Figure A6. (a) Comparison between $\text{C III } 0.97\mu\text{m}/\text{He II } 1.01\mu\text{m}$ and $\text{C IV } 1.19\mu\text{m}/\text{He II } 1.16\mu\text{m}$ ratios for WN/C stars (diamonds), WC (triangles) and broad-lined WN stars (squares) plus newly identified WC stars (filled circles). (b) Comparison between $\text{C IV } 2.07\mu\text{m}/(\text{C III} + \text{He I} + \text{N III } 2.11\mu\text{m})$ ratios. Symbols are the same as panel (a).

In the Y-band, we consider a range of diagnostic ratios to discriminate between WC subtypes. Fig. A7(a) compares $\text{C III } 1.20\mu\text{m}/\text{C IV } 1.19\mu\text{m}$ to $\text{C II } 0.99\mu\text{m}/\text{C III } 0.97\mu\text{m}$ for late (WC8-9, triangles), mid (WC6-7, diamonds) and early (WC4-5, squares) subtypes. The former cleanly separates WC8 and WC9 stars from earlier subtypes, but fails to discriminate between WC4-7 stars and is severely hindered by severe blending in broad lined systems which are common at early subtypes. Similarly, the latter separates WC9 and

WC7-8 from earlier subtypes, but $\text{C II } 0.99\mu\text{m}$ is extremely weak at early subtypes (absent at WC4) and lies in the electron scattering wing of $\text{C III } 0.97\mu\text{m}$ for broad-lined stars.

Helium lines are not generally considered when visually classifying WC stars, since the strongest features are severely blended with carbon lines, e.g. $\text{He II } 4686\text{\AA}$ ($\text{He I } 5876\text{\AA}$) lies in the wing of $\text{C III } 4650\text{\AA}$ ($\text{C IV } 5808\text{\AA}$). However, in the Y-band, $\text{He II } 1.01\mu\text{m}$ is relatively isolated – albeit with a C IV contribution – and $\text{He I } 1.08\mu\text{m}$ is prominent through-

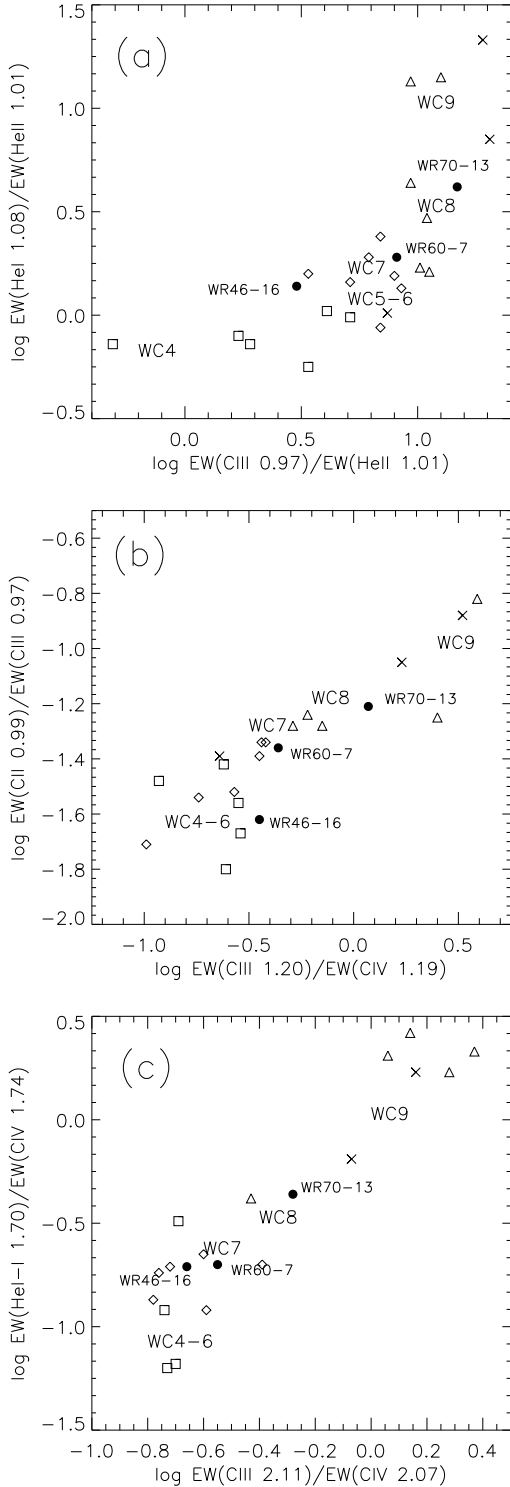


Figure A7. (a) Comparison between C III 1.20 μ m/C IV 1.19 μ m and C II 0.99 μ m/C III 0.97 μ m ratios for WC8–9 stars (triangles), WC6–7 stars (diamonds), WC4–5 stars (squares) plus newly identified WC stars (filled circles) and newly classified WC stars WR75aa, WR75c and WR107a (crosses); (b) Comparison between C III 0.97 μ m/He II 1.01 μ m and He I 1.08 μ m/He II 1.01 μ m ratios for WC stars, symbols as above; (c) comparison between C III 2.11 μ m/C IV 2.07 μ m and He I–II 1.70 μ m/C IV 1.74 μ m ratios for WC stars, symbols as above.

out the WC sequence. Therefore, Fig. A7(b) compares C III 0.97 μ m/He II 1.01 μ m to He I 1.08 μ m/He II 1.01 μ m for late, mid and early subtypes. The former separates WC4 stars from later subtypes, owing to a ratio of <1 , and also discriminates between WC6–7 and WC8–9 stars at a ratio of ~ 10 . The latter ratio maps reasonably well onto the WC sequence, especially for WC9 (>10) and WC4 (<1) subtypes.

Fig. A7(c) compares the ratio of the strongest carbon lines in the K-band, C III 2.11 μ m/C IV 2.07 μ m, with the ratio of the (He II 1.69 μ m + He I 1.70 μ m)/C IV 1.74 μ m. For WC4–7 stars the latter is effectively the ratio of the helium-to-carbon recombination lines (12–7 transition for helium, 9–8 transition for carbon), so will depend upon the C/He ratio as well as ionization. In contrast, the 1.7 μ m helium feature is dominated by He I 1.70 μ m in WC8 and especially WC9 subtypes, so this represents a better ionization indicator for late subtypes. The K-band diagnostic cleanly separates WC4–7 subtypes from WC8 and WC9 stars, but fails to distinguish between early subtypes, as has previously been shown (Eenens et al. 1991; Figer et al. 1997). The H-band diagnostic also distinguishes between WC8 and WC9 stars, but also maps earlier WC subtypes reasonably well. C II 1.78 μ m is also prominent at late subtypes, such that C II 1.785 μ m/C IV 1.736 > 1 in WC9 subtypes.

A4 WO stars

At visual wavelengths, strong O VI 3818 \AA emission discriminates WO stars from early WC stars, with ratios of O VI to O V 5590 \AA and/or C VI 5808 \AA providing WO subclasses Crowther et al. (1998). The majority of known WO stars have been observed in the near-IR (this work, Tramper et al. 2015). Unfortunately, the sole ionization stage of oxygen present in the near-IR spectrum of WO stars is O VI (1.075 μ m, 1.458 μ m, 1.917 μ m, 2.463 μ m), preventing discrimination between WO subtypes, plus the exceptionally broad lines of WO stars leads to severe blending in most spectral regions.

Nevertheless, beyond their line widths, WO stars present a highly distinctive near-IR appearance. They can be distinguished from WC4 stars by the presence of O VI features, with high O VI 1.075 μ m/C IV 1.190 μ m and O VI 1.46 μ m/C IV 1.40 μ m ratios, although 1.46 μ m is severely blended with C IV 1.43 μ m and He II 1.47 μ m in most WO stars, and 1.075 μ m is blended with He I 1.083 μ m. He IV LH41-1042 Neugent et al. (2012); Tramper et al. (2015) is unambiguously characterized as a WO star from the presence of O VI features, although C III 0.97 μ m is prominent at this (WO4) subtype. Since O VI lines are weak, WO stars also exhibit unusually weak helium lines with respect to early WC stars, such that WO stars possess He II 1.16/C IV 1.19 ≤ 0.2 , versus ~ 0.5 – 0.6 in WC4 subtypes (recall Fig. A1). In addition, C III 0.97 μ m and C IV 2.07 μ m are weak in WO3 stars and absent in WO2 stars.

Table A1. Near-IR equivalent width and FWHM measurements for optically classified Galactic WN stars. Equivalent widths (in Å) are generally robust to ± 0.05 dex, except for weak lines ± 0.1 dex, while measured FWHM (in km s^{-1}) are generally reliable to $\pm 50 \text{ km s}^{-1}$ (approximate values are indicated with colons). The key to the spectroscopic datasets utilised is provided in Table 2.

WR	WN SpType	Ref	He II 1.01 FWHM $\log W_\lambda$	He I 1.08 $\log W_\lambda$	P_γ $\log W_\lambda$	N v 1.11 $\log W_\lambda$	He II 1.16 $\log W_\lambda$	$P\beta$ $\log W_\lambda$	He II 1.48 $\log W_\lambda$	N v 1.55 $\log W_\lambda$	He II 1.69 $\log W_\lambda$	He I 1.70 $\log W_\lambda$	He I 2.06 $\log W_\lambda$	N III-v 2.11 $\log W_\lambda$	Br γ $\log W_\lambda$	He II 2.19 FWHM $\log W_\lambda$	Note	Data			
WR3	WN3(h)	S96	2470	2.13	<0	0.9:	0.8				1.23	0.2:		0.90	1.43	2580	1.75	2.11 \ll 2.10	O1,U3		
WR6	WN4b	S96	2500	2.63	— 2.60 —		2.30	2.02	2.18	0.8:	1.43	1.46		1.53	1.76	2160	2.20	2.11 \sim 2.10	I1,M1		
WR8	WN7o/CE	S96	1480	2.13	2.58	1.43		1.99	1.89	1.72	0.8	1.59	1.15	2.0:	1.92	1.76	1350	1.73	2.11 \ll 2.07	U2,N6	
WR10	WN5ha	S96	1480	2.03	1.26	1.2:	0.5:	1.66	1.81	1.5:		1.2:	<0.0		0.3:	1.48	1250	1.63	2.11 \ll 2.19	N3	
WR18	WN4b	S96	3020	2.65	2.39	1.6:		2.34	1.99	2.00	0.9	1.75	1.1:		1.4:	1.56	3100	2.23	2.11 \sim 2.10	N6	
WR24	WN6ha	S96	1510	1.72	1.48			1.33	1.52						0.88	1.57	1500:	1.46	2.11 \ll 2.19	N3	
WR26	WN4-6b/CE	S96	2920	2.66	2.59	1.1		2.43	2.02	2.12	0.7	1.74	1.48		1.90	1.69	3040	2.24	2.11 \ll 2.07	N6	
WR40	WN8h	S96	1070	1.55	2.58	1.66		1.36	1.91	1.0			0.5:	1.71	1.41	1.58	1.98	1180	1.16	2.11 \gg 2.19	N6
WR46	WN3b pec	S96	2750	2.41	<0.6						1.38	1.5:	<0.9		1.20	1.45	2920	2.10	2.11 \ll 2.10	E1,N6	
WR51	WN4o	S96	1790	2.38	1.77	1.31	0.80	2.06	1.75	1.83	0.90				1.41	1.61	1600	1.85	2.11 \sim 2.10	N2	
WR54	WN5o	S96	1600	2.39	2.01	1.45	0.95	2.13	1.78	1.88	0.78				1.41	1.59	1700	1.88	2.11 \sim 2.10	N2	
WR55	WN7o	S96	1270	2.03	2.47	1.4		1.89	1.73				0.6:		1.56	1.76	1310	1.63	2.11 \sim 2.19	N2	
WR61	WN5o	S96	1640	2.41	2.13	1.36	0.7:	2.15	1.73	1.89	0.78				1.43	1.54	1490	1.85	2.11 $>$ 2.10	N2	
WR66	WN8h	S86	1330	1.72	2.30	1.36		1.61	1.74	1.34			0.9:		1.45	1.64	1330	1.27	2.11 \gg 2.19	N2	
WR75	WN6b	S96	2780	2.56	2.83	1.1:	1.1:	2.30	2.06				0.8:		1.66	1.86	2700	2.02	2.11 \gg 2.10	N2	
WR77sc	WN7b	C06	3100	2.48	2.97	1.3:		2.29	2.02	2.01	0.7	1.5:	1.9:		1.76	1.88	2840	2.08	2.11 $<$ 2.19	N5	
WR78	WN7h	S96	1100	1.80	2.01	1.27		1.58	1.63				1.0:	1.1:	0.9:	1.23	1.58	1630	1.45	2.11 \sim 2.19	N6
WR82	WN7(h)	S96	1120	1.90	2.46	1.74		1.80	2.03	1.46			0.6:		1.48	1.78	860	1.36	2.11 \sim 2.19	N2	
WR83	WN5o	S96	1540	2.28	1.96	1.46	0.8:	2.07	1.79	1.80	0.8				1.36	1.72	1520	1.85	2.11 $>$ 2.10	N2	
WR84	WN7o	S96	1240	2.13	2.40	1.36		2.00	1.72	1.73			0.7:		1.52	1.60	1040	1.63	2.11 $<$ 2.19	N2	
WR87	WN7h+a	S96	1150	1.46	1.64	1.0:		1.20	1.63	0.99										2.11 \sim 2.19	N2
WR89	WN8h+a	S96	960	1.3	1.67	0.9:		1.15	1.52	0.89					1.18	1.52	740	0.85	2.11 \sim 2.19	N2	
WR98	WN8o/C7	S96	1400	1.83	2.55	1.45		1.80	1.83	1.53			1.20		1.78	1.74	1080	1.90	2.11 $>$ 2.07	N5	
WR105	WN9h	S96	500	0.88	2.27	1.38	1.30	0.3:	1.76				<0.0	1.36	1.68	1.43	1.84	160	-0.2:	2.11 \gg 2.19	U5,U6
WR108	WN9ha	S96	400	0.92	1.68	0.83			1.32						1.28	1.34	170	-0.3:	2.11 \gg 2.19	U3,U4	
WR110	WN5-6b	S96	3500	2.64	2.81	1.3:	1.3:	2.37	2.06	2.13	1.0:				1.55	1.88	3200	2.02	2.11 \gg 2.10	U3	
WR115	WN6o	S96	1260	2.48	2.51	1.25	0.2:						1.28	1.36		1.52	1.54	1160	1.76	2.11 $<$ 2.19	U3
WR116	WN8h	S96	830	1.32	2.68	1.78		1.18	2.08	0.7:			2.04		1.54	1.90	1100:	0.7	2.11 \gg 2.19	U3,U4	
WR120	WN7o	S96	970	1.86	2.51	1.31		1.76	1.76	1.50			1.1:		1.68	1.68	1050	1.54	2.11 \sim 2.19	U3,U4	
WR123	WN8o	S96	930	1.60	2.68	1.56		1.52	1.85	1.06			1.73		1.78	1.87	930	1.38	2.11 \gg 2.19	U3,U4	
WR128	WN4(h)	S96	1900	2.24	1.41	1.32	1.04		1.75				1.36	0.6:		1.28	1.58	1750	1.87	2.11 \ll 2.10	U3
WR131	WN7h+a	S96	1000	1.68	1.59	1.13			1.48				0.9:	0.5:		0.95	1.50	1040	1.20	2.11 $<$ 2.19	U3
WR134	WN6b	S96	2690	2.60	2.54	1.64	1.0:		2.01				1.73	1.36:		1.50	1.69	2560	2.10	2.11 $>$ 2.10	U3
WR136	WN6b(h)	S96	1920	2.48	2.51	1.77	0.7:	2.25*	2.05				1.68	1.41:		1.59	1.91	1800	2.03	2.11 \gg 2.10	U3
WR138	WN5-6o	C11	1440	2.03	1.79	1.18	0.2:		1.54				1.28	0.7:		1.25	1.56	1450	1.76	2.11 $>$ 2.10	U3
WR145	WN7o/CE	S96	1520	2.01	2.25	1.1			1.58				1.34	1.30	0.7:	1.54	1.59	1510	1.71	2.11 $>$ 2.07	U3
WR152	WN3(h)	S96	1980	2.31	1.23	1.35	0.97						1.43	0.5:		1.18	1.59	1950	1.96	2.11 \ll 2.10	U3

S90: (Smith et al. 1990); C06: (Crowther et al. 2006), C11: (Crowther & Walborn 2011), * W.D.Vacca (priv. comm.)

Note: 2.10 = N v 2.100; 2.11 = He I 2.112 + N III 2.116; 2.19 = He II 2.189

Table A2. Near-IR equivalent width and FWHM measurements for visually classified Magellanic Cloud WN stars (LMC: BAT#, SMC: AB#). Equivalent widths (in Å) are generally robust to ± 0.05 dex, except for weak lines ± 0.1 dex, while measured FWHM (in km s^{-1}) are generally reliable to $\pm 50 \text{ km s}^{-1}$ (approximate values are indicated with colons). The key to the spectroscopic datasets utilised is provided in Table 2. Several sets of measurements are provided for the variable LBV + WN star AB5 (HD 5980).

WR	WN	Ref	He II 1.01	He I 1.08	P γ	N v 1.11	He II 1.16	P β	He II 1.48	N v 1.55	He II 1.57	Note	Data	
	SpType		FWHM $\log W_\lambda$	$\log W_\lambda$	$\log W_\lambda$	$\log W_\lambda$	$\log W_\lambda$	$\log W_\lambda$	$\log W_\lambda$	$\log W_\lambda$	$\log W_\lambda$			
BAT1	WN3b	F03b	2050	2.75	1.08	1.36	0.9:	2.34	1.84	2.08	0.9:	1.43		N4
BAT2	WN2b(h)	F03b	2680	2.48	<1.0			2.13	1.65	1.9:			He I 1.08 absent	N4
BAT3	WN4b	F03b	1920	2.55	2.32	1.5:	<0.8	2.22	1.81	1.98	0.8:			N4
BAT5	WN2b	F03b	2430	2.56	<1.0	1.1:	1.0:	2.20	1.66	1.9			He I 1.08 absent	N4
BAT7	WN4b	F03b	3900	2.88	1.97	1.60		2.44	2.06	2.18		1.85		N4
BAT16	WN8h	S96	950	1.67	2.38	1.60		1.54	1.95	1.1:				N3
BAT17	WN4o	F03b	1780	2.29	2.22	1.23	0.8:	2.01	1.63	1.76	0.8:	1.1	$\log(\text{N v } 1.55/\text{He II } 1.57) = 0$	N3
BAT18	WN3(h)	F03b	1770	2.35	1.69	1.47	0.5	2.06	1.80	1.87		1.0:		N4
BAT24	WN4b	F03b	2610	2.68	2.56	1.55	<0.8	2.34	1.94	2.12	0.8:			N4
BAT25	WN4ha	F03b	1580	1.96	<0.7	1.1		1.68	1.60	1.53	0.9:			N4
BAT30	WN6h	S96	970	1.91	1.93	1.65		1.76	1.76	1.43		0.9:		N3
BAT31	WN4b	F03b	1860	2.49	2.29	1.4	0.6:	2.22	1.76	1.98		1.3		N4
BAT37	WN3o	F03b	1770	2.53	1.81	1.33	0.7:	2.25	1.80	2.05	0.9:	1.3		N4
BAT47	WN3o‡	F03b	1640	2.61	1.75	1.49	0.95	2.33	1.86	2.11	0.9:	1.4		N4
BAT51	WN3b	F03b	3020	2.65	1.72	1.59	0.5:	2.42	1.90	2.14		1.3		N3,N4
BAT60	WN4(h)a	F03b	1840	1.99	1.15	1.03	0.3	1.77	1.56	1.56				N4
BAT66	WN3(h)	F03b	1840	2.32	<0.8	1.3:	0.6	2.03	1.76	1.83				N4
BAT67	WN5ha	F03b	1720	2.01	1.43	1.2		1.70	1.53	1.43				N4
BAT75	WN4o	F03b	1730	2.46	2.08	1.53		2.18	1.73	1.90		1.1		N4
BAT76	WN9h	C95	370	0.66	2.12	1.30							$\log(\text{Br}\gamma/\text{He II } 2.189) = +1.5$	C1
BAT77	WN7ha	S08	890	1.12	1.55	1.4:		1.08	1.55					N3
BAT78	WN4(h)	W99	1590	1.61	1.23	1.1:		1.56	1.40	1.38				N3
BAT88	WN4b/CE	F03b	2670	2.75	2.54	1.69		2.46	1.93	2.20		1.54	$\log(\text{C IV } 1.19/\text{He II } 1.16) = -0.9$	N4
BAT89	WN7h	S96	1040	1.93	2.35	1.60		1.81	1.88	1.43		1.0		N3
BAT92	WN6+B11a	M86	1000	1.76	2.27	1.22		1.53	1.72	1.32				N4
BAT117	WN5ha	F03b	2350	1.99	1.1:	1.23		1.70	1.57	1.45				N4
BAT118	WN6h	S96	1340	2.05	2.08	1.50		1.78	1.81	1.45		0.8		N3
BAT119	WN6(h)	S96	1460	2.01	1.99	1.34		1.74	1.71	1.43				N4
BAT122	WN5(h)	F03b	1510	2.13	1.67	1.56		1.85	1.76	1.68		1.0		N3
BAT134	WN4b	F03b	1960	2.62	2.53	1.41		2.32	1.90	2.05		1.48		N4
AB1	WN3ha	F03a	1550	1.88	<0.0	0.78		1.53	1.38	1.4:			He I 1.08 absent	N3,N4
AB2	WN5ha	F03a	1020	1.56	0.9:	0.7:		1.1:	1.28					N4
AB4	WN6h	F03a	1070	1.94	1.45	1.20		1.61	1.61	1.41		0.9	$\log(\text{Br}\gamma/\text{He II } 2.189) = -0.08$	N1
AB5			1160	2.00	2.31	1.58		1.82	1.81	1.63		1.1	Sep 99	N1
AB5			2040	2.13	2.10	1.45		1.89	1.77	1.73		1.3	Nov 03	N3
AB5			1500	2.10	2.06	1.37		1.89	1.76	1.65		1.0:	Nov 04	N4

M86: (Moffat & Seggewiss 1986), C95: (Crowther et al. 1995a), S96: (Smith et al. 1996), W99 (Walborn et al. 1999), F03a (Foellmi et al. 2003a), F03b (Foellmi et al. 2003b), S08: (Schnurr et al. 2008)

‡We adopt WN3o for BAT47 on the owing to its modest FWHM ($\ll 1900 \text{ km/s}$) whereas Foellmi et al. (2003b) adopted WN3b.

Table A3. Near-IR equivalent width and FWHM measurements for visually classified WC and WO stars in the Milky Way and Magellanic Clouds. Equivalent widths (in Å) are generally robust to ± 0.05 dex, except for weak lines ± 0.1 dex, while measured FWHM (in km s^{-1}) are generally reliable to $\pm 50 \text{ km s}^{-1}$ (approximate values are indicated with colons). The key to the spectroscopic datasets utilised is provided in Table 2

WR	WC SpType	Ref	C III 0.97 log W_λ	C II 0.99 log W_λ	He II 1.01 FWHM	He II 1.01 log W_λ	He I 1.08 log W_λ	He II 1.16 log W_λ	C IV 1.19 log W_λ	C III 1.20 log W_λ	C IV 1.43 log W_λ	He I-II 1.70 log W_λ	C IV 1.74 FWHM	C IV 1.74 log W_λ	C II 1.78 log W_λ	He I 2.06 log W_λ	C IV 2.07 log W_λ	C III 2.11 log W_λ	C IV 2.43 log W_λ	Data
WR4	WC5	S90					2.20					1.70	2360	2.62			3.20	2.46		U3
WR5	WC6	S90					2.38					1.76	1950	2.47					2.56	U3
WR14	WC7	S90	2.94	1.42	1960	2.10	2.48	2.05	2.24	1.67	2.21	1.72	2150	2.43	1.6:		3.01	2.29	2.47	N3
WR15	WC6	S90	2.91	1.2:	3300	2.38	2.58	2.21	2.44	1.45	2.05	1.53	3060	2.40			3.04	2.26	2.50	N6
WR23	WC6	S90	2.94	1.40	2490	2.23	2.39	2.13	2.40	1.66	2.25	1.59	2620	2.51			3.09	2.50	2.57	N6
WR52	WC4-5	C98	2.84	1.36	2460	2.31	2.06	2.08	2.49	1.56	2.38:	1.38	2560	2.58			3.22	2.49	2.70	N2,N6
WR56	WC7	S90	3.06	1.72	1810	2.13	2.26	2.03	2.29	1.87	2.33					2.81	2.23		N2	
WR57	WC8	S90	3.10	1.82	1590	2.05	2.26	1.99	2.23	1.94	2.26					2.42	1.96		N2	
WR60	WC8	S90	3.09	1.85	2260	2.05	2.52	2.00	2.26	2.04	2.29					2.63	2.36		N2	
WR64	WC7	S90	3.08	1.74	1840	2.24	2.18	2.03	2.33	1.89	2.35					2.81	2.26		N2	
WR88	WC9	S90	2.45	1.20	900	1.48	2.61	1.49	1.40	1.80	1.56	1.77	1060	1.46	1.61	1.75	1.99	2.05	1.18	N6
WR90	WC7	S90	2.96	1.57	2170	2.17	2.45	2.08	2.30	1.85	2.15:	1.75	2310	2.40			3.07	2.47	2.44	N6
WR92	WC9	S90	2.50	1.68	800	1.40	2.55	1.62	1.43	2.02	1.68	1.72	1050	1.30	1.96	2.22	1.85	1.99	1.11	N6
WR101	WC8	L89	3.00	1.72	2230	1.99	2.22	2.03	2.26	2.11	2.38									N5
WR103	WC9d	S90					2.49					1.51	900	1.28	1.88	1.94	1.50	1.78		U3
WR111	WC5	S90	2.98:	1.41	2320	2.27	2.26					1.41	2250	2.59	1.2:		3.23	2.53	2.66	I1,U1,U3
WR114	WC5	S90	2.94	1.52	2350	2.33	2.35	2.16	2.43	1.79	2.25					2.94	2.20			N2
WR121	WC9d	S90					2.47					1.25	930	0.92	1.53	1.66	1.04	1.41	0.5:	U3
WR135	WC8	S90	2.86	1.52	1270	1.89	2.53					1.80	1450	2.18	1.70		2.74	2.31	2.15	I1,U1,U3
WR137	WC7d+O	S90	2.56	1.34	1660	1.66	1.85									2.67	2.06			I1,L1
WR140	WC7d+O	S90														2.69	2.30			L1
WR143	WC4	S90														3.10	2.37	2.65		U3
WR146	WC4-5+O	C98					2.23					1.61	3200	2.10		2.80	2.11	2.23		U3
WR154	WC6	S90					2.36					1.80	2360	2.54		3.12	2.36			U3
BAT9	WC4	S90	2.27	<0.6	2890	2.58	2.44	2.33	2.43	1.89	2.05									N4
BAT11	WC4	S90	2.70	<0.9	3710	2.47	2.37	2.20	2.40	1.79	2.13									N3
BAT121	WC4	B01	2.76	<1.2	3260	2.48	2.34	2.20	2.44	1.89	2.09									N4
WR	WO SpType	Ref	C III 0.97 log W_λ	He II 1.01 FWHM	He II 1.01 log W_λ	C IV 1.05 log W_λ	O VI 1.07 log W_λ	He I 1.08 log W_λ	He II 1.16 log W_λ	C IV 1.19 log W_λ	C IV 1.40 log W_λ	C IV 1.43 log W_λ	O VI 1.46 log W_λ	He II 1.48 log W_λ	C IV 1.74 FWHM	C IV 1.74 log W_λ	C IV 2.07 log W_λ	C IV 2.10 log W_λ	C IV 2.43 log W_λ	Data
WR93b	WO3	C98		5800	2.69	1.98	2.04		2.04	2.86	2.58	1.9:	1.9:	1.8:	5060	2.92		2.21	3.20	N5
WR102	WO2	C98		6600	2.50	1.74	2.22		1.5:	2.79	2.65	–	– 2.32 –	–	5890	2.83		2.09	3.05	N5
WR142	WO2	C98		7100	2.67	1.3	1.8			2.8					6700	2.86		1.95	3.0	V1
BAT123	WO3	C98		4200	2.74	1.95	1.93		2.14	2.79		– 2.0 –	–	3650	2.93			3.2	3.16	V1
LH41-1042	WO4	N12	2.05	4200	2.71	1.78	2.03	1.7:	2.13	2.88		2.2:	2.1:	2.2:	3650	2.97	3.08	3.1	3.18	V1
AB8	WO3+O	C98	≤ 1.3	3200	1.78	1.2:	1.3:		1.81	2.34					3750	2.54		2.8:	2.9	V1

L89: (Lundstrom & Stenholm 1989), S90: (Smith et al. 1990); C98: (Crowther et al. 1998); B01: (Bartzakos et al. 2001); N12: (Neugent et al. 2012)

REFERENCES

- Bartzakos P., Moffat A. F. J., Niemela V. S., 2001, *MNRAS*, **324**, 18
- Conti P. S., Leep M. E., Perry D. N., 1983, *ApJ*, **268**, 228
- Crowther P. A., Smith L. J., 1996, *A&A*, **305**, 541
- Crowther P. A., Walborn N. R., 2011, *MNRAS*, **416**, 1311
- Crowther P. A., Hillier D. J., Smith L. J., 1995a, *A&A*, **293**, 172
- Crowther P. A., Hillier D. J., Smith L. J., 1995b, *A&A*, **293**, 403
- Crowther P. A., Smith L. J., Hillier D. J., 1995c, *A&A*, **302**, 457
- Crowther P. A., De Marco O., Barlow M. J., 1998, *MNRAS*, **296**, 367
- Crowther P. A., Hadfield L. J., Clark J. S., Negueruela I., Vacca W. D., 2006, *MNRAS*, **372**, 1407
- Eenens P. R. J., Williams P. M., Wade R., 1991, *MNRAS*, **252**, 300
- Figer D. F., McLean I. S., Najarro F., 1997, *ApJ*, **486**, 420
- Foellmi C., Moffat A. F. J., Guerrero M. A., 2003a, *MNRAS*, **338**, 360
- Foellmi C., Moffat A. F. J., Guerrero M. A., 2003b, *MNRAS*, **338**, 1025
- Hainich R., et al., 2014, *A&A*, **565**, A27
- Hamann W.-R., Gräfener G., Liermann A., 2006, *A&A*, **457**, 1015
- Lundstrom I., Stenholm B., 1989, *A&A*, **218**, 199
- Moffat A. F. J., Seggewiss W., 1986, *ApJ*, **309**, 714
- Neugent K. F., Massey P., Morrell N., 2012, *AJ*, **144**, 162
- Schnurr O., Moffat A. F. J., St-Louis N., Morrell N. I., Guerrero M. A., 2008, *MNRAS*, **389**, 806
- Smith L. F., Shara M. M., Moffat A. F. J., 1990, *ApJ*, **358**, 229
- Smith L. F., Shara M. M., Moffat A. F. J., 1996, *MNRAS*, **281**, 163
- Tramper F., et al., 2015, *A&A*, **581**, A110
- Walborn N. R., Drissen L., Parker J. W., Saha A., MacKenty J. W., White R. L., 1999, *AJ*, **118**, 1684

**APPENDIX B: SPECTROSCOPIC
OBSERVATIONS OF IR SELECTED
CANDIDATES**

This paper has been typeset from a $\text{\TeX}/\text{\LaTeX}$ file prepared by the author.

Table B1. Catalogue of candidates spectroscopically observed with NTT/SOFI, indicating emission (em) or absorption (abs) line features.

ID	l	b	RA	Dec	J	H	K	[3.6]	[4.5]	[5.8]	[8.0]	Notes
			J2000		mag	mag	mag	mag	mag	mag	mag	
E#3	298.0981	-0.3769	12:08:52.47	-62:50:54.9	13.34	11.67	10.47	9.67	9.21	8.92	8.49	WR46-18 (WC6-7)
E#2	298.1901	-0.4807	12:09:31.38	-62:57:57.7	14.98	13.40	12.21	11.13	10.76	10.48	10.05	-
E#4	298.5476	-0.4541	12:12:40.16	-62:59:43.7	13.56	12.41	11.56	10.76	10.45	10.12	9.85	-
E#1	298.9823	+0.3429	12:17:23.44	-62:14:16.3	14.47	13.07	12.08	11.12	10.74	10.43	10.15	Br γ em
B#3	300.4069	+0.0016	12:29:20.63	-62:45:42.1	13.27	10.66	9.09	8.07	7.55	7.05	6.99	Br γ abs
B#6	300.7404	-0.2304	12:32:05.88	-63:01:11.4	14.40	13.29	12.57	11.86	11.46	11.18	11.05	Weak Br γ em
D#1	302.1241	-0.2318	12:44:17.82	-62:05:32.8	12.78	11.45	10.64	9.75	9.44	9.06	8.85	Br γ , 10, 11, He I 2.058 em
B#9	302.1126	+0.4871	12:44:22.22	-62:22:24.0	15.62	13.80	12.75	11.81	11.40	11.11	10.94	weak Br γ em
B#13	302.8599	+0.4606	12:50:48.98	-62:24:39.8	13.32	12.92	11.09	10.39	9.95	9.70	9.40	WR47-5 (WN6(h))
B#15	303.8459	+0.0727	12:59:26.03	-62:47:05.4	14.64	12.90	11.65	10.32	9.89	9.55	9.15	-
B#18	304.2777	-0.3314	13:03:22.21	-63:10:19.4	15.18	13.51	12.59	12.08	11.60	11.18	10.97	Weak Br γ em
B#21	304.7418	-0.4276	13:07:31.72	-63:14:34.3	13.33	10.85	9.35	7.61	7.02	6.78	6.36	CO 2.3 abs
A#1	305.2360	+0.0224	13:11:35.63	-62:45:32.6	15.98	14.01	12.64	11.04	10.58	10.11	9.72	-
A#2	305.2674	+0.2222	13:11:43.79	-62:33:26.9	16.07	13.24	11.33	9.25	8.62	8.07	7.70	-
B#22	305.2689	-0.1301	13:11:59.17	-62:54:30.9	13.66	12.43	11.60	11.08	10.68	10.18	9.76	Br γ , 10, 11 em
B#26	305.6698	-0.0117	13:15:23.76	-62:45:21.7	12.99	11.69	10.83	9.96	9.56	9.23	9.03	Br γ , 10, 11 em
B#27	305.7340	-0.3132	13:16:12.44	-63:03:00.6	15.14	13.87	12.93	12.16	11.67	11.37	11.13	Weak Br γ em
B#28	305.7956	-0.2272	13:16:40.46	-62:57:30.8	16.19	13.99	12.50	10.54	10.03	9.67	9.49	-
B#30	305.9956	+0.0635	13:18:09.56	-62:38:56.7	15.17	13.34	12.16	11.11	10.63	10.25	9.86	-
A#4	306.0554	-0.0271	13:18:45.64	-62:43:59.1	13.62	11.65	10.17	8.67	8.15	7.71	7.36	-
B#31	306.4620	-0.2216	13:22:29.34	-62:52:49.3	15.01	13.17	12.15	11.10	10.68	10.44	10.29	-
B#33	306.7893	+0.2640	13:24:47.24	-62:21:27.7	15.58	13.27	11.74	9.85	9.34	9.00	8.47	-
D#2	307.2723	-0.1744	13:29:27.72	-62:43:31.3	12.87	11.60	10.82	10.00	9.67	9.32	9.02	Br γ , 10, 11 em
B#36	308.2364	-0.1775	13:37:44.90	-62:34:16.9	14.58	13.21	12.38	11.48	11.01	10.76	10.64	-
B#38	308.7720	+0.3908	13:41:21.77	-61:54:48.5	14.40	12.84	11.87	10.91	10.50	10.32	10.08	Br γ , 10, 11 em
B#37	308.7434	-0.0387	13:41:50.01	-62:20:25.8	14.94	13.21	12.18	11.31	10.83	10.66	10.49	WR56-1 (WN5o)
B#40	309.0157	+0.0950	13:43:53.90	-62:09:19.5	16.18	13.84	12.53	11.33	10.92	10.54	10.25	-
B#41	309.0367	-0.4150	13:44:58.44	-62:39:01.8	15.42	13.66	12.46	10.96	10.48	10.13	9.69	-
B#42	309.2191	+0.0369	13:45:42.37	-62:10:13.7	14.66	13.37	12.53	11.72	11.29	10.99	10.63	-
A#5	309.8974	+0.3827	13:50:41.49	-61:41:06.3	14.79	12.97	11.61	10.22	9.73	9.26	8.71	-
B#45	310.2014	-0.3327	13:54:38.45	-62:18:32.7	15.29	13.03	11.62	10.48	10.03	9.74	9.46	Br γ , 10, 11 em
B#46	310.2641	-0.1602	13:54:48.21	-62:07:35.6	14.29	12.89	12.07	11.34	10.93	10.62	10.33	-
B#47	310.3786	-0.0643	13:55:33.11	-62:00:20.0	14.00	12.71	11.85	11.15	10.71	10.30	10.11	Weak Br γ em
B#48	310.6160	-0.3828	13:58:12.06	-62:15:15.7	13.78	12.27	11.34	10.53	10.03	9.79	9.53	Br γ em
B#50	311.1224	+0.2097	14:01:02.41	-61:33:00.6	13.91	12.45	11.53	10.70	10.28	9.88	9.59	Br γ , 10, 11 em
B#51	311.3533	+0.3626	14:02:33.44	-61:20:27.2	13.28	11.57	10.28	9.19	8.76	8.46	8.18	WR60-7 (WC7-8)
B#52	311.3750	+0.1595	14:03:11.73	-61:31:49.2	15.82	13.61	12.34	11.20	10.76	10.48	10.25	Br γ , 10, 11 em
A#6	311.4747	-0.4529	14:05:26.94	-62:05:27.2	15.34	13.69	12.57	11.25	10.85	10.62	10.33	-
B#54	312.1913	-0.1538	14:10:31.18	-61:35:44.4	16.19	13.08	11.25	9.93	9.50	9.19	8.94	Br γ abs
B#57	312.4077	+0.3376	14:11:00.14	-61:03:42.5	15.09	12.71	11.37	10.12	9.64	9.27	9.04	Br γ , He I 2.058 em
B#55	312.2737	-0.2463	14:11:24.98	-61:39:31.9	15.51	13.54	12.34	11.33	10.80	10.58	10.44	Br γ em
B#56	312.3518	-0.3278	14:12:15.19	-61:42:45.2	14.90	12.98	11.76	10.61	10.10	9.72	9.43	WR60-8 (WN6o)
B#58	312.8095	+0.4991	14:13:44.39	-60:47:04.4	16.43	14.09	12.65	10.88	10.23	9.85	9.52	-
B#59	313.0292	+0.1771	14:16:17.64	-61:01:12.4	11.57	10.49	9.81	9.37	8.63	8.62	8.38	Br γ , 10, 11, He I 2.058 em
B#60	313.2705	-0.0194	14:18:42.65	-61:07:37.6	15.10	13.60	12.70	11.74	11.30	11.01	10.87	Br γ em
C#6	313.8298	+0.0804	14:22:46.4	0 -60:50:38.7	11.86	10.57	9.80	8.93	8.61	8.32	8.10	Br γ , 10, 11, He I 2.058 em
A#7	314.2797	+0.4370	14:25:11.50	-60:21:09.6	14.85	11.98	10.10	8.18	7.73	7.26	6.99	-
C#3	314.0615	-0.3361	14:25:46.13	-61:09:10.4	12.93	11.79	11.04	10.31	9.95	9.68	9.41	Br γ , 10, 11 em
B#66	314.9795	+0.0376	14:31:39.06	-60:28:07.2	15.99	14.17	13.03	12.81	12.28	11.92	11.38	He I 2.058 em
B#65	314.9262	-0.3702	14:32:30.51	-60:51:58.6	13.93	12.63	11.85	11.17	10.63	10.52	10.24	Br γ , 10, 11 em
B#69	316.1646	+0.1717	14:39:59.99	-59:52:52.5	14.95	13.57	12.72	11.81	11.31	10.92	10.78	-
C#13	316.6186	-0.4678	14:45:26.51	-60:16:28.3	13.72	12.51	11.74	11.07	10.73	10.45	10.12	Br γ , 10, 11 em
B#72	317.1176	+0.2706	14:46:31.62	-59:23:37.5	14.91	13.18	12.02	10.61	10.06	9.74	9.49	-
B#75	317.4918	-0.3007	14:51:09.26	-59:44:40.5	15.29	13.19	11.96	10.59	9.95	9.51	9.33	-
B#76	317.6899	+0.0868	14:51:11.84	-59:18:33.8	14.56	12.66	11.37	10.21	9.70	9.41	8.76	-
B#78	318.0224	+0.0688	14:53:35.11	-59:10:35.3	15.31	13.24	11.80	10.41	9.92	9.62	9.46	-
B#80	318.3162	-0.0265	14:55:57.84	-59:07:38.1	15.57	13.12	11.49	9.74	9.08	8.65	8.18	-
B#82	318.4866	+0.0168	14:56:59.05	-59:00:36.7	15.77	13.67	12.35	10.81	10.26	9.94	9.53	-
B#81	318.4855	+0.0116	14:56:59.74	-59:00:54.8	16.09	13.62	12.14	10.93	10.39	10.09	9.90	-
B#83	318.5683	+0.0024	14:57:35.91	-58:59:05.8	15.18	13.34	12.15	11.25	10.75	10.47	10.28	Br γ , 10, 11 em
B#84	318.7320	+0.2431	14:57:51.03	-58:41:44.6	16.37	14.29	13.05	12.12	11.59	11.11	10.55	-
B#86	319.1429	+0.2102	15:00:45.20	-58:31:52.1	13.21	12.01	11.32	10.80	10.35	10.10	9.86	Br γ , 10, 11 em
B#85	319.0607	-0.0724	15:01:14.05	-58:49:07.4	14.46	12.88	11.89	10.82	10.31	10.13	9.76	WR64-2 (WN6o)

Table B1. (continued)

ID	l	b	RA	Dec	J	H	K	[3.6]	[4.5]	[5.8]	[8.0]	Notes
			J2000		mag	mag	mag	mag	mag	mag	mag	
B#87	319.4120	+0.1536	15:02:46.14	-58:27:06.5	12.39	11.04	10.18	9.30	8.83	8.68	8.34	WR64-3 (WN6o)
B#88	319.5721	+0.0601	15:04:11.15	-58:27:21.5	11.35	10.01	9.10	8.34	7.88	7.68	7.41	WR64-4 (WN6o+OB)
B#91	320.0540	+0.0209	15:07:31.84	-58:15:09.6	13.11	11.66	10.80	9.91	9.47	9.25	8.97	WR64-5 (WN6o)
B#93	320.5939	+0.0474	15:10:57.65	-57:57:28.5	13.84	12.19	11.11	10.12	9.58	9.31	8.97	WR64-6 (WN6b)
B#95	320.7930	-0.4404	15:14:09.21	-58:16:26.9	15.93	13.87	12.66	11.58	11.12	10.68	10.52	Br γ em
C#34	321.1822	-0.0202	15:15:00.68	-57:42:46.0	14.10	12.67	11.76	10.85	10.48	10.18	9.89	Br γ , 10, 11 em
B#96	322.1468	-0.3860	15:22:33.62	-57:30:26.4	12.67	10.52	9.07	7.48	6.91	6.42	6.09	Br γ em
B#100	323.5860	-0.2326	15:30:42.92	-56:34:38.5	12.52	11.21	10.35	9.46	9.00	8.80	8.51	CO 2.3 abs
B#103	324.3283	+0.1597	15:33:28.03	-55:49:48.0	13.16	11.93	11.13	10.46	10.03	9.87	9.63	broad Br γ , 10, 11 em
B#106	324.6980	+0.2691	15:35:09.10	-55:31:34.7	14.67	12.98	11.97	10.87	10.42	10.17	9.91	-
B#105	324.6326	-0.4487	15:37:46.51	-56:08:45.2	13.12	11.38	9.96	8.44	7.94	7.59	7.38	WR70-13 (WC8d)
B#107	324.9946	-0.3129	15:39:17.02	-55:49:18.9	14.12	12.58	11.50	10.35	9.76	9.58	9.22	WR70-14 (WN4b)
C#44	326.2077	+0.4099	15:43:02.30	-54:30:55.8	13.01	11.74	10.94	10.11	9.76	9.38	9.12	Br γ em?
B#110	326.6728	+0.4761	15:45:17.55	-54:10:46.9	15.51	13.57	12.37	10.93	10.39	10.03	9.56	-
C#48	326.0985	-0.3665	15:45:43.54	-55:11:51.5	12.84	11.42	10.49	9.55	9.17	8.84	8.57	Br γ , 10, 11 em
B#116	328.3669	+0.2962	15:54:59.19	-53:15:35.4	15.58	13.51	12.20	11.29	10.76	10.48	10.29	Br γ em
B#118	328.5562	-0.0472	15:57:26.19	-53:24:05.3	14.09	12.28	11.12	9.93	9.42	9.11	8.95	broad Br γ , 10, 11 em
B#119	328.6291	-0.0897	15:57:59.60	-53:23:12.5	16.18	14.25	13.08	12.02	11.56	11.20	11.08	-
B#123	329.1414	+0.2865	15:58:57.97	-52:46:05.4	15.61	13.59	12.40	11.20	10.62	10.34	10.12	WR70-15 (WN5o)
B#125	329.3266	+0.2204	16:00:10.73	-52:41:51.6	12.97	11.48	10.57	9.75	9.30	9.08	8.89	Br γ , 10, 11 em
B#122	328.9764	-0.4398	16:01:17.50	-53:25:34.2	14.70	12.69	10.74	9.37	8.87	8.40	8.16	CO 2.3 abs
B#127	329.4091	+0.0227	16:01:26.78	-52:47:35.7	15.56	13.41	12.11	11.01	10.50	10.23	9.86	broad Br γ em
B#124	329.1877	-0.4186	16:02:15.92	-53:16:16.7	15.22	13.43	12.26	10.61	10.16	9.88	9.62	-
B#130	330.1017	+0.3914	16:03:16.34	-52:03:34.6	13.74	12.49	11.69	10.96	10.54	10.27	10.01	Br γ , 10, 11 em
C#29	330.8606	+0.4416	16:06:43.15	-51:31:01.9	15.03	13.17	11.78	10.33	9.86	9.53	9.08	-
B#133	330.6085	+0.1173	16:06:54.91	-51:55:36.9	14.33	12.85	11.95	10.91	10.52	10.28	10.11	Br γ , 10, 11 em
B#132	330.5909	+0.0726	16:07:01.45	-51:58:18.3	12.56	11.14	10.27	9.50	8.98	8.74	8.46	WR72-5 (WN6o)
B#134	330.6751	+0.1604	16:07:02.83	-51:51:00.7	15.53	13.58	12.40	11.28	10.88	10.66	10.42	Br γ em
B#131	330.3175	-0.2612	16:07:09.70	-52:24:09.7	14.75	12.76	11.45	10.23	9.72	9.29	9.11	-
B#135	330.7968	+0.2625	16:07:11.27	-51:41:34.2	13.56	12.11	11.24	10.31	9.77	9.60	9.22	-
C#31	331.0646	+0.3349	16:08:09.05	-51:27:33.2	14.20	12.76	11.90	11.03	10.64	10.33	10.07	Br γ , 10, 11 em
C#46	331.2770	+0.3320	16:09:10.09	-51:19:04.9	11.97	10.66	9.86	9.00	8.61	8.33	8.06	Br γ , 10, 11, He I 2.058 em
B#136	331.1094	+0.0024	16:09:48.50	-51:40:26.7	13.53	12.03	11.16	10.49	10.07	9.84	9.65	Br γ , 10, 11 em
B#137	331.2573	+0.1529	16:09:51.13	-51:27:47.3	15.48	13.60	12.46	11.69	11.23	10.81	10.81	Br γ em
A#9	330.7901	-0.4539	16:10:17.68	-52:13:33.6	12.63	11.10	9.95	8.60	8.16	7.78	7.56	Br γ em
B#138	331.4221	-0.0219	16:11:23.45	-51:28:45.6	15.71	13.70	12.43	11.31	10.82	10.34	10.31	Br γ , 10 em
C#36	331.2588	-0.2259	16:11:31.09	-51:44:23.8	12.68	11.48	10.80	10.35	10.04	9.69	9.12	-
B#139	332.1603	-0.3519	16:16:16.61	-51:20:40.5	13.76	12.38	11.49	10.65	10.26	10.00	9.83	Br γ , 10, He I 2.058 em
A#10	332.7911	+0.0695	16:17:17.67	-50:28:11.5	14.34	12.30	10.96	9.41	8.93	8.48	8.27	Br γ em
B#140	333.6774	+0.3817	16:19:52.89	-49:37:37.1	15.71	13.71	12.51	11.15	10.51	10.37	10.09	-
B#141	333.6899	-0.1793	16:22:23.37	-50:00:56.8	15.90	13.85	12.60	11.27	10.63	10.34	9.86	-
C#38	334.4312	+0.2406	16:23:46.34	-49:11:37.7	13.09	12.02	11.37	10.78	10.37	10.38	9.90	Br γ em
A#11	334.7557	+0.2255	16:25:13.60	-48:58:22.3	15.28	13.34	12.21	11.12	10.66	10.38	10.10	WR75-31 (WN7o)
B#143	334.8115	+0.1094	16:25:58.25	-49:00:50.7	15.05	13.15	12.03	10.91	10.50	10.22	9.97	Br γ , 10, 11 em
B#145	335.4017	+0.3561	16:27:23.18	-48:25:06.4	14.78	13.20	12.26	11.29	10.84	10.56	10.25	-
B#144	335.0446	-0.4287	16:29:19.69	-49:13:09.3	15.87	13.91	12.56	11.16	10.60	10.21	9.77	-
B#147	335.4470	-0.1581	16:29:49.32	-48:44:28.2	14.73	13.18	12.23	11.27	10.80	10.60	10.36	broad Br γ , 10, 11 em
C#41	336.2729	+0.2343	16:31:30.87	-47:52:16.2	13.68	12.32	11.48	10.66	10.32	9.98	9.70	Br γ , 10, 11 em
A#12	336.2983	+0.1534	16:31:58.23	-47:54:28.5	15.66	13.74	12.50	11.28	10.81	10.38	10.40	Br γ , 10, 11 em
A#13	336.3959	+0.1395	16:32:25.70	-47:50:45.8	15.15	12.93	11.57	10.35	9.75	9.54	9.35	WR75-30 (WN7o)
C#39	336.4792	-0.4420	16:35:19.23	-48:10:46.5	11.53	10.42	9.77	9.16	8.64	8.49	8.20	Br γ , He I 2.058 em
B#148	337.2407	+0.1689	16:35:41.65	-47:12:19.4	14.98	13.15	11.89	10.38	9.67	9.31	9.06	-
B#149	337.4217	+0.1337	16:36:33.84	-47:05:42.9	15.12	13.10	11.89	10.91	10.49	10.17	9.98	broad Br γ , 10, 11 em
C#33	337.5172	+0.1107	16:37:02.50	-47:02:24.0	13.90	12.40	11.52	10.43	10.09	9.80	9.56	Br γ , 10, 11, He I 2.058 em
B#150	337.7587	-0.0231	16:38:34.35	-46:57:00.2	14.61	12.56	11.12	9.61	9.13	8.74	8.61	Br γ , 10, 11, He I 2.058 em
B#151	337.9344	-0.1758	16:39:55.49	-46:55:14.6	14.95	12.85	11.56	10.48	9.98	9.57	9.44	Br γ , 10, 11, He I 2.058 em
B#152	337.9619	-0.1518	16:39:55.61	-46:53:03.2	14.31	12.31	10.85	9.32	8.77	8.28	7.89	-
B#154	338.5451	+0.2997	16:40:12.92	-46:08:54.0	15.05	13.15	11.98	10.88	10.43	10.10	9.97	WR76-11 (WN7o)
B#153	338.2202	-0.1241	16:40:48.38	-46:40:21.0	13.61	11.68	10.48	8.85	8.29	7.75	7.76	CO 2.3 abs
B#155	338.9494	-0.0691	16:43:21.24	-46:05:16.5	15.14	13.20	12.03	10.90	10.48	10.13	9.97	Br γ , 10, 11, He I 2.058 em
B#156	339.1638	+0.0831	16:43:30.11	-45:49:34.6	14.04	12.46	10.85	9.13	8.66	8.24	8.31	-
C#43	338.9622	-0.4951	16:45:15.96	-46:21:24.7	12.93	11.81	11.03	10.21	9.88	9.61	9.37	Br γ , 10, 11, He I 2.058 em
B#157	339.8284	-0.0272	16:46:27.58	-45:23:40.3	14.96	13.29	12.10	10.92	10.47	10.04	9.94	Br γ , 10, 11, He I 2.058 em
C#42	339.3198	-0.4615	16:46:27.72	-46:03:48.1	12.91	11.73	10.94	10.16	9.84	9.51	9.25	Br γ , 10, 11 em